JGR Space Physics

RESEARCH ARTICLE
10.1029/2025JA033825

MHD Simulations of Europa's Interaction With Jupiter's Magnetosphere During the Juno Flyby: Electron Beams in the Plasma Wake

S. Cervantes[1,2], J. Saur[1], S. Duling[1], J. R. Szalay[3], S. Schlegel[1], J. E. P. Connerney[4,5], F. Allegrini[6,7], and S. Bolton[6]

[1]Institute of Geophysics and Meteorology, University of Cologne, Cologne, Germany, [2]Astronomy & Astrophysics Section, School of Cosmic Physics, Dublin Institute for Advanced Studies, DIAS Dunsink Observatory, Dublin, Ireland, [3]Department of Astrophysical Sciences, Princeton University, Princeton, NJ, USA, [4]Space Research Corporation, Annapolis, MD, USA, [5]NASA Goddard Space Flight Center, Greenbelt, MD, USA, [6]Southwest Research Institute, San Antonio, TX, USA, [7]Department of Physics and Astronomy, University of Texas at San Antonio, San Antonio, TX, USA

Abstract In September 2022, the Juno mission performed its only close flyby of Europa and traversed the moon's wake at a minimum distance of ~350 km. Among other findings, the Jovian Auroral Distributions Experiment (JADE) detector onboard the spacecraft discovered intense field-aligned electron beams (~30–300 eV) downstream of the moon. In this study, we apply a three-dimensional magnetohydrodynamic model to simulate the plasma interaction of Jupiter's magnetosphere with Europa and its atmosphere for the conditions of this flyby, and we specifically focus on the influence of the electron beams on the plasma density and the magnetic field in the moon's space environment. We include these beams in our simulations as sheets of locally enhanced ionization, and we use electron impact ionization rates of O_2 derived from JADE electron measurements to characterize the sheets. We compare our results with the magnetic field and the total ion number density measurements from Juno's magnetometer and JADE detector, respectively. Our results show that the beams fill the wake downstream of Europa with newly ionized plasma, and that they generate large variations in the magnetic field which contribute partially to the observed magnetic field. Our study demonstrates that the electron beams are critical factors in shaping Europa's magnetic field and plasma environment, and thus they need to be accounted for in the data analysis of the upcoming JUICE and Europa Clipper missions.

Key Points:

- We include electron beams, an asymmetric O_2 atmosphere, and non-uniform ionization in our magnetohydrodynamic simulations of the Juno flyby at Europa
- We investigate the effect of the enhanced ionization due to the electron beams on the plasma density and magnetic field around Europa
- We show that the beams fill the wake and generate magnetic field perturbations which contribute to the observed magnetic field

Supporting Information:

Supporting Information may be found in the online version of this article.

Correspondence to:

S. Cervantes,
scervantes@cp.dias.ie

Citation:

Cervantes, S., Saur, J., Duling, S., Szalay, J. R., Schlegel, S., Connerney, J. E. P., et al. (2025). MHD simulations of Europa's interaction with Jupiter's magnetosphere during the Juno flyby: Electron beams in the plasma wake. *Journal of Geophysical Research: Space Physics*, *130*, e2025JA033825. https://doi.org/10.1029/2025JA033825

Received 7 FEB 2025
Accepted 10 JUN 2025

1. Introduction

The interaction of magnetospheric plasma flowing at sub-Alfvénic velocities past an orbiting moon is a common phenomenon in the outer planets of the Solar System (e.g., M. Kivelson et al., 2004; Saur, 2021). Such a sub-Alfvénic interaction is experienced by Jupiter's moon Europa, since the Jovian plasma and magnetic field nearly corotate with the planet, and the plasma constantly overtakes the moon from its trailing hemisphere. As a consequence, the local plasma environment is modified through ionization and collisions within Europa's atmosphere. The resulting perturbations of the plasma flow and magnetic field propagate as Alfvén waves away from the moon, forming a tube-shaped region known as the Alfvén wing (Goertz, 1980; Neubauer, 1980, 1998). Furthermore, induced fields in Europa's interior also perturb the plasma flow and magnetic field environment near the moon (Neubauer, 1999; Volwerk et al., 2007).

Between 1996 and 2000, the Galileo spacecraft made eight flybys close to Europa and obtained in situ magnetic field and plasma measurements. A wide variety of numerical simulations has been performed in order to provide context for the data collected by Galileo and to understand the interaction between Europa's atmosphere and the magnetospheric plasma (e.g., Harris et al., 2021; Kabin et al., 1999; Rubin et al., 2015; Saur et al., 1998). These modeling studies have focused on several aspects of the interaction, for example, induced fields from Europa's subsurface ocean (Schilling et al., 2007, 2008), the effect of localized water plumes (Arnold et al., 2019; Blöcker et al., 2016; Jia et al., 2018), or the influence of a stable water component around the subsolar point on the moon's trailing hemisphere (Cervantes & Saur, 2022).

A recent flyby performed by the Juno mission (Bolton et al., 2017) on 29 September 2022 discovered bi-directional, magnetic-field-aligned electron beams with energies from ~30 to 300 eV downstream of Europa (Allegrini et al., 2024a). These observations revealed a new, previously unknown mechanism of the complex

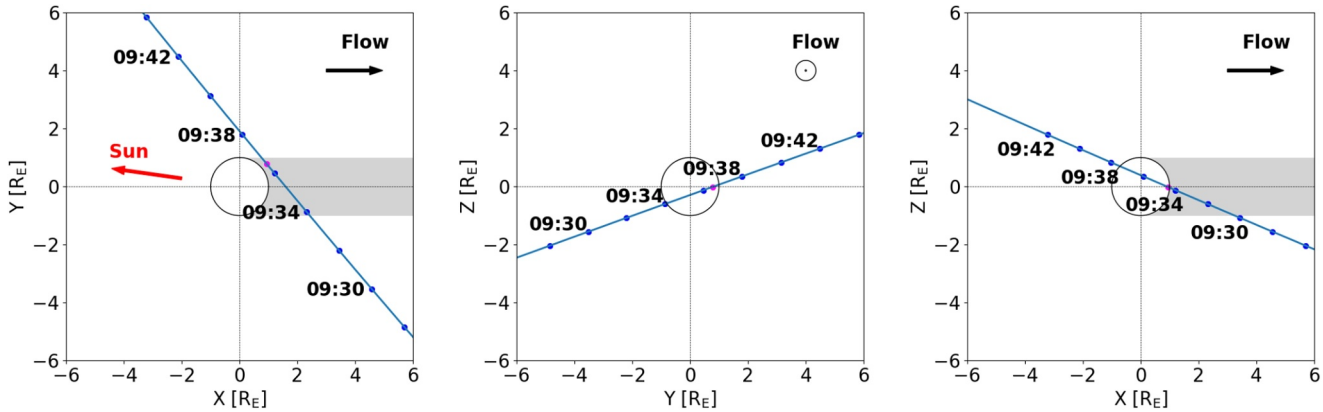

Figure 1. Trajectory of the Juno flyby at Europa in the EPhiO coordinate system in the *XY* (left), *YZ* (middle), and *XZ* (right) planes. The times (in UTC) associated with Juno's position are labeled on the trajectories. The point in magenta marks the position of closest approach. The gray shaded region indicates Europa's downstream geometric wake.

interaction between the moon's atmosphere and the Jovian magnetospheric plasma. Similar electron beams, also related to moon-magnetosphere interaction, had already been detected near Io in Galileo spacecraft measurements (Frank & Paterson, 1999; Williams et al., 1996). These electron beams were observed downstream and over the poles of Io at energies between ∼100 eV and ∼30 keV, which, however, are higher than the energies of the newly discovered electron beams at Europa. As Allegrini et al. (2024a) shows, the beams locally enhance electron impact ionization in Europa's atmosphere by more than a factor of three over the local space environment, and they are associated with large variations in the magnetic field. In addition, by using the measured pitch angle distribution, the authors constrain their likely origin to be near or within Jupiter's plasma disk.

The geometry of Juno's encounter with Europa is shown in Figure 1 in the EPhiO coordinate system, where the primary direction *Z* is parallel to Jupiter's spin axis, the secondary direction *Y* points towards Jupiter, and the *X* axis completes the right-handed system along the direction of the corotational plasma flow. Juno approached Europa from the downstream, anti-Jovian side, while traveling northward, and encountered the moon at a minimum altitude of 354 km close to Europa's equatorial plane at 09:36:29 UTC. Juno traversed the geometric wake behind the moon between 09:34:06 and 09:36:47 UTC, and then continued its trajectory heading northward towards Jupiter. At the time of the flyby, Europa was located above the Jovian plasmasheet at a magnetic latitude of 4.1° and a System III longitude of 136.2°W.

The purpose of our study is to investigate how the electron beams influence Europa's plasma interaction. We apply a single-fluid magnetohydrodynamic (MHD) model and simulate the interaction between Europa's atmosphere and the Jovian plasma for the conditions of the Juno flyby. We analyze two data sets returned by the Juno spacecraft during its encounter with Europa: (a) the magnetic field recorded by the magnetometer (Connerney et al., 2017), and (b) plasma density measurements from the Jovian Auroral Distributions Experiment (JADE) detector (McComas et al., 2017). The comparison between our MHD simulation results and the spacecraft data allows us to investigate whether certain perturbations in the magnetic field and plasma observations can be explained by the enhanced ionization due to the presence of electron beams downstream of Europa. Other possible effects of the beams which might also contribute to the observed magnetic field perturbations, for example, by carrying electric current, are not accounted for in our model and are outside of the scope of our study.

Our work is based on two published papers which also examine magnetic field and plasma data from this same Juno encounter: (a) the above-mentioned study by Allegrini et al. (2024a); and (b) Szalay et al. (2024), which among several findings, reports observations of O_2^+ pickup ions at Europa, estimates the production rate of O_2 within the moon's surface, and presents a timeseries of total ion number density and electron impact ionization rate of O_2 along the trajectory of Juno. Furthermore, we would like to emphasize the study by Addison et al. (2024) who also model the magnetometer measurements during the Juno flyby with a hybrid code. The authors explain the observed magnetic field signatures with a highly asymmetric atmosphere and a deviation of the corotational plasma flow. We will discuss the differences between our work and Addison et al. (2024) in Sections 2.3 and 3.

This manuscript is organized in the following way. In Section 2, we present the single-fluid MHD model for Europa's interaction with the Jovian magnetosphere, and we describe our implementation of the field-aligned electron beams. In Section 3, we show the results of our MHD simulations for different scenarios of the plasma interaction, and in Section 4, we discuss our findings. Finally, Section 5 summarizes the most important results and presents some concluding remarks.

2. Magnetohydrodynamic Model

We describe the interaction between Europa's atmosphere and the ambient magnetospheric plasma with a three-dimensional (3D) single-fluid MHD model, based on an MHD model adjusted to moon-magnetosphere interaction in Duling et al. (2022). We use a Cartesian and a spherical coordinate system, both centered at Europa. The Cartesian system is the EPhiO system, as described in Section 1. The spherical coordinate system is characterized by the radius r, the colatitude θ measured from the positive Z axis, and the longitude ϕ measured from the positive Y axis in direction to the negative X axis.

For our numerical simulations we employ a spherical grid with $160 \times 120 \times 240$ (r, θ, ϕ) cells. The model domain extends to 20 R_E from the moon's center in radial direction. The radial resolution is not equidistant and it stretches gradually from cell to cell from the inner to the outer boundary. The resolution at the surface of Europa is chosen to be 12 km. The angular resolution of the grid is equidistant in θ with $\Delta\theta = 1.5°$. The angular resolution in ϕ is not equidistant. In the upstream hemisphere ($X < 0,\ \phi \leq 180°$), the grid consists of 60 cells with $\Delta\phi = 3°$, whereas in the downstream hemisphere ($X > 0,\ \phi > 180°$), it consists of 180 cells with $\Delta\phi = 1°$.

2.1. MHD Model Equations

In our single-fluid MHD model the plasma interaction between Europa's atmosphere and Jupiter's magnetosphere is described by the following four variables: magnetic field $\mathbf{B}$, plasma bulk velocity $\mathbf{v}$, plasma mass density ρ, and total thermal pressure p. The MHD evolution equations for each of these variables read:

$$\frac{\partial \rho}{\partial t} + \nabla \cdot (\rho \mathbf{v}) = P m_n - L m_L, \tag{1}$$

$$\frac{\partial \rho \mathbf{v}}{\partial t} + \nabla \cdot \left[\rho \mathbf{v}\mathbf{v} - \frac{1}{\mu_0}\mathbf{B}\mathbf{B} + \mathbf{I}\left(p + \frac{1}{2}\frac{B^2}{\mu_0}\right)\right] = -(L m_L + \nu_n \rho)\,\mathbf{v}, \tag{2}$$

$$\frac{\partial \mathbf{B}}{\partial t} - \nabla \times (\mathbf{v} \times \mathbf{B}) = 0, \tag{3}$$

$$\begin{aligned} \frac{\partial E_t}{\partial t} + \nabla \cdot \left[\left(E_t + p + \frac{1}{2}\frac{B^2}{\mu_0}\right)\mathbf{v} - \frac{1}{\mu_0}\mathbf{B}(\mathbf{v}\cdot\mathbf{B})\right] = &-\frac{1}{2}(L m_L + \nu_n \rho)\, v^2 - \frac{3}{2}(L m_L + \nu_n \rho) \\ &\frac{p}{\rho} + \frac{3}{2}(P m_n + \nu_n \rho)\,\frac{k_B T_n}{m_n}. \end{aligned} \tag{4}$$

with plasma production and loss rates P and L, respectively, ion-neutral collision frequency ν_n, and total energy $E_t = \frac{1}{2}\rho v^2 + \frac{3}{2}p + \frac{1}{2}\frac{B^2}{\mu_0}$ as the sum of the kinetic, thermal, and magnetic energy. In the last term of the right hand side of the energy Equation 4, T_n corresponds to the temperature of the neutral atmosphere, which we set to 130 K, as in Blöcker et al. (2016).

In our model, singly charged O_2^+ ions are produced, and we assume the mass of O_2 molecules $m_n = m_L = 32$ u. The quantitative expressions for the plasma production and loss rates and the collision frequency are specified in Section 2.2.

The Jovian background magnetic field at the location of Europa is obtained by excluding the perturbed values of the Juno magnetometer data around 20 min of closest approach (CA), performing a linear fit, and extracting the fitted values at CA. This results in a background field $\mathbf{B}_0 = (70,\ -120,\ -420)$ nT. We consider a plasma bulk velocity $v_0 = 100$ km s^{-1} in the corotation direction. Based on Juno's JADE measurements, we adopt an upstream plasma number density of 100 cm^{-3} from Szalay et al. (2024). This value is within the range of 50–150 cm^{-3} for the magnetospheric electron density surrounding Europa derived from measurements by the

Juno Waves instrument (Kurth et al., 2017) and presented in Kurth et al. (2023). We assume an average ion mass $\widetilde{m}_i = 18.5$ u for the upstream magnetospheric plasma (M. Kivelson et al., 2004), resulting in an upstream mass density of $\rho_0 = 1.85 \times 10^9$ u m^{-3}. Similar to other studies, we consider an upstream thermal pressure $p_0 = 4.8$ nPa (M. Kivelson et al., 2004).

2.2. Plasma Sources and Losses

We include electron impact ionization and photo ionization as source terms of the plasma mass density in Equation 1. The production rate for the combined effect of both processes is calculated with:

$$P = \nu_{\text{ion}} n_n, \tag{5}$$

with total ionization frequency $\nu_{\text{ion}} = \nu_{\text{ei}} + \nu_{\text{ph}}$, where ν_{ei} and ν_{ph} are the electron impact ionization and photo ionization rates, respectively, and n_n is the corresponding neutral O_2 number density.

We distinguish between two electron populations that contribute to ionization by impacts on the neutral O_2 atmosphere: the background magnetospheric electrons and the field-aligned electron beams. We prescribe the electron impact ionization rates to produce O_2^+ arising from these two distinct populations with different models, which are presented in further detail in Section 2.4. Similar to Rubin et al. (2015), we assume a photo ionization rate to produce O_2^+ of $\nu_{\text{ph}} = 1.7 \times 10^{-8}$ s^{-1} from Huebner et al. (1992), and we apply it everywhere except in the shadow cast by Europa.

Dissociative recombination between ions and electrons is the sink of plasma particles in our model. We parameterize this process with a recombination rate coefficient $\alpha = 2.5 \times 10^{-14}$ m^{3}s^{-1} for O_2^+ assuming an ionospheric electron temperature of 0.5 eV, as given by Schunk and Nagy (2009). In analogy to Duling et al. (2022) and Saur et al. (2003), we avoid that the plasma mass density decreases below the upstream value ρ_0 by adopting the following expression:

$$L = \begin{cases} \alpha\rho(\rho - \rho_0)\, m_L^{-2} & , \quad \text{for } \rho > \rho_0 \\ 0 & , \quad \text{for } \rho < \rho_0 \end{cases}. \tag{6}$$

We implement the exchange of momentum due to particle collisions between ions and neutrals by introducing the ion-neutral collision frequency:

$$\nu_n = \sigma_n v_0 n_n, \tag{7}$$

with ion-neutral collision cross section σ_n. We adopt an O_2 cross section of 2.2×10^{-19} m^{-2} similar to Saur et al. (1998), Cervantes and Saur (2022), and Duling et al. (2022). The momentum transfer cross section accounts for both induced dipole ion-molecule interactions and charge exchange.

2.3. Neutral Atmosphere

In this study, we consider two analytical expressions for Europa's molecular oxygen atmosphere. First, we apply a radially symmetric description of the global atmosphere, with number density given as:

$$n_{O_2}(h) = n_{O_2,0} \cdot \exp\left(-\frac{h}{H_{O_2}}\right), \tag{8}$$

with scale height $H_{O_2} = 100$ km, surface number density $n_{O_2,0} = 10^{13}$ m^{-3}, altitude $h = r - R_E$ above the surface, and Europa's radius $R_E = 1569$ km. This results in a uniform column density $N_{O_2} = 10^{18}$ m^{-2} around the moon. This column density agrees with trends from the recent literature which have shown that low column densities of O_2 are needed for consistency with existing observations (e.g., Cervantes & Saur, 2022; Roth, 2021).

In the second description, we prescribe Europa's atmosphere with a sub-Jovian/anti-Jovian asymmetry. We decrease the neutral O_2 density by 50% in the sub-Jovian apex compared to the anti-Jovian apex. For this, we multiply Equation 8 with a coefficient dependent on the longitude ϕ:

$$n_{O_2}(h,\phi,\theta) = \left\{0.5 + \left[0.5\ \sin^2\left(\frac{\phi}{2}\right)\right]\cdot \sin(\theta)\right\}\cdot n_{O_2,0}\cdot \exp\left(-\frac{h}{H_{O_2}}\right). \quad (9)$$

The colatitude-dependent term $\sin(\theta)$ ensures that there is no discontinuity of the number density over the poles in our atmospheric model. The resulting profile is symmetric with respect to the YZ plane of our coordinate system, with minimum column density $N_{O_2} = 5 \times 10^{17}$ m^{-2} for $\phi = 0°$ (i.e., the Jupiter facing meridian) and maximum column density $N_{O_2} = 10^{18}$ m^{-2} for $\phi = 180°$.

As shown in Figure 1, at the time of the encounter, the subsolar point was located ~8° in longitude away from the upstream apex towards Jupiter. This implies that the dusk and the dawn hemispheres approximately corresponded to the anti-Jovian ($Y < 0$) and the sub-Jovian hemispheres ($Y > 0$), respectively. Therefore, our modeled sub-Jovian/anti-Jovian asymmetry roughly coincides with a dawn/dusk asymmetry in Europa's atmosphere.

Spectral telescope images provide a means to study properties (e.g., composition, structure, etc.) of a planetary body's atmosphere remotely, and possibly, to infer the presence of any asymmetry in its distribution. Roth et al. (2016) analyzed a set of 20 Hubble Space Telescope (HST) aurora observations of Europa's atmosphere and found that the right-hand side hemisphere in the images showed brighter emissions (with a surplus of >50%) compared to the left-hand side hemisphere with only a few exceptions. The authors suggested that such a right-left asymmetry could arise due to atmospheric changes with local time in Europa, since the brighter right hemisphere is the dusk hemisphere and the fainter left hemisphere is the dawn side. In a later study, Roth (2021) reanalyzed nine sets of HST images from Roth et al. (2016), and reported an asymmetry by a factor of ~2 between the oxygen emission ratio r_γ(OI) of the dawn and the dusk sides of Europa, which could be explained by a surplus of O_2 on the dusk hemisphere compared to the dawn hemisphere. This factor is similar to the ratio of 2 between the column densities at the anti-Jovian and the sub-Jovian apexes in the profile given by Equation 9. However, it must be emphasized that the conclusions from Roth (2021) were drawn from images taken in visits from 1999, 2012, and 2015, and not at the time of the Europa flyby. Simultaneous observations of HST during Juno's CA to the moon would have provided evidence for the presence of any dawn/dusk asymmetry at Europa, but they were not performed, as the passage of HST in the area of the South Atlantic Anomaly impeded them. Nevertheless, since the asymmetry in r_γ(OI) reported by Roth (2021) was observed at three different epochs, this might be a persistent feature in the moon's atmosphere, and thus we consider such a dawn/dusk (ca. sub-Jovian/anti-Jovian) asymmetry to be a plausible scenario. Finally, it is worth mentioning that in a recent MHD modeling work, Addison et al. (2024) also treat Europa's atmosphere as dawn/dusk asymmetric with a bulge of O_2 centered around the anti-Jovian apex, albeit with an analytical expression different than the one in our study. Their resulting atmospheric column densities range uses a much stronger asymmetry from 2.5×10^{13} m^{-2} to 5×10^{18} m^{-2}, at the sub-Jovian and anti-Jovian apexes, respectively.

2.4. Electron Impact Ionization

The implementation of electron impact ionization of O_2 in our MHD model warrants a more detailed description. As mentioned in Section 2.2, we assume that the total electron impact ionization frequency (ν_{ei}) stems from two contributions: ionization by the background magnetospheric electrons ($\nu_{ei,0}$) and ionization by the electron beams downstream of Europa ($\nu_{ei,beams}$). The ionization frequencies in our model are informed by: (a) the electron impact ionization rates of O_2 derived from JADE electron measurements (Szalay et al., 2024), and (b) modeling studies of the electron temperature in Europa's plasma environment (Blöcker et al., 2016; Saur et al., 1998).

2.4.1. Background Ionization Frequency

We apply two descriptions for the background ionization frequency. In the first one, we assume a constant frequency of $\nu_{ei,0} = 4.6 \times 10^{-6}$ s^{-1}, which corresponds to the nominal upstream value during the Juno flyby, as presented by Szalay et al. (2024). We apply this ionization frequency uniformly over the whole domain, as displayed in panel (a) of Figure 2.

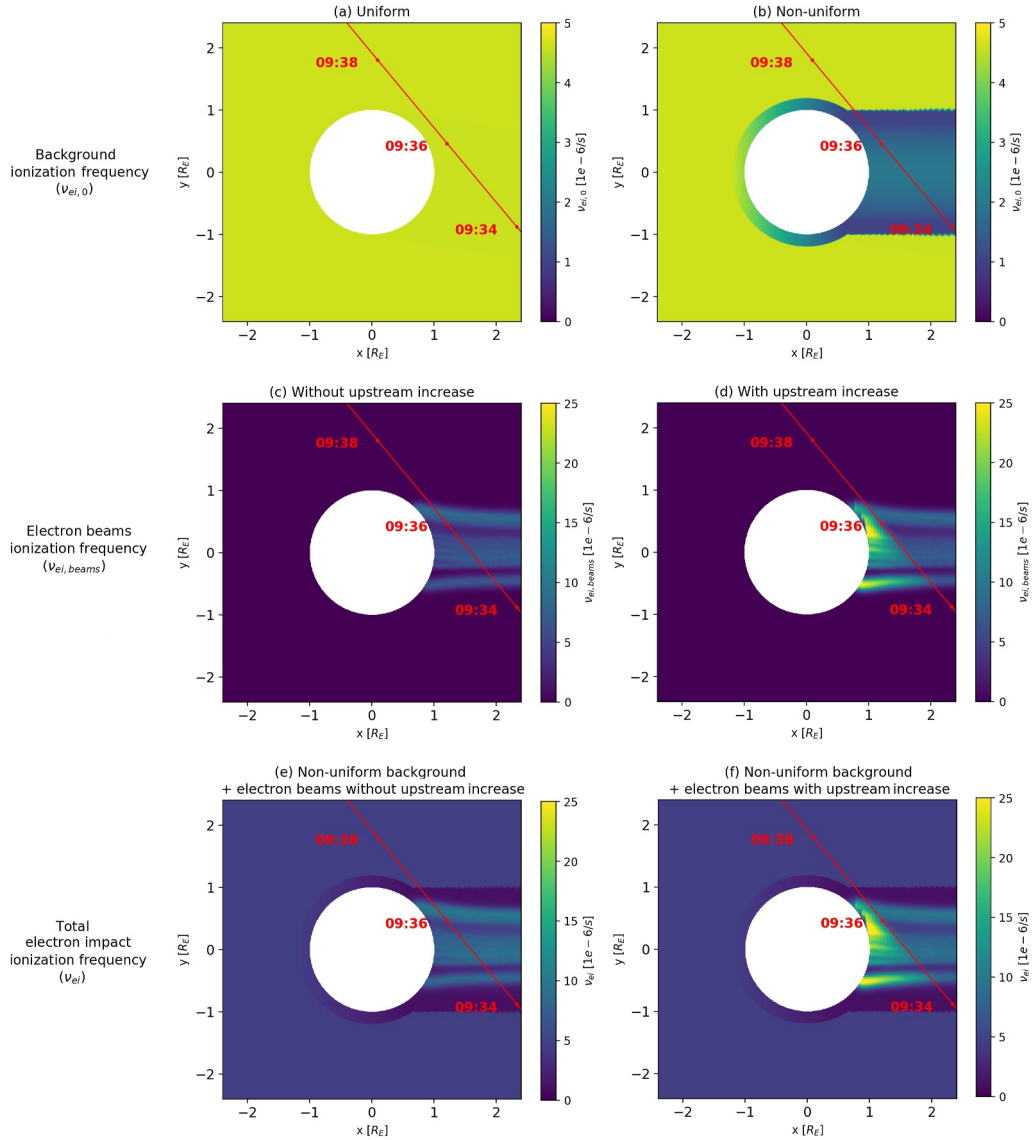

Figure 2. Electron impact ionization frequency in the equatorial plane: (a) uniform background, (b) non-uniform background, (c) electron beams without upstream increase in ionization, (d) electron beams with upstream increase in ionization, (e) non-uniform background plus electron beams without upstream increase in ionization (i.e., (b) + (c)), (f) non-uniform background plus electron beams with upstream increase in ionization (i.e., (b) + (d)). Note that the limits of the color bar are different before (a–b) and after including electron beams (c–f). The red line shows Juno's flyby trajectory projected onto this plane. Panels (a) and (b) refer to the scenarios described in Section 2.4.1, and panels (c) to (f) refer to steps (7) and (8) in Section 2.4.2.

Our second description assumes a non-uniform background ionization frequency. Electron impact ionization depends strongly on the temperature of the impinging electrons (Blöcker et al., 2016; Saur et al., 1998). Magnetospheric electrons that undergo inelastic collisions with Europa's neutral atmosphere are cooled down, and as they are advected downstream, the ionization frequency in the wake is reduced. In line with the results from Saur et al. (1998), we include this effect in our model by assuming an upstream ionization frequency of $\nu_{\mathrm{ei},0} = 4.6 \times 10^{-6}\ \mathrm{s}^{-1}$, and decreasing it around Europa and throughout its wake according to the following equations:

$$\nu_{ei,0} = \begin{cases} 10^{-6} + 2\times10^{-6}\cdot(0.6 - X) \quad s^{-1} & , \quad -1.15\ R_E < X < 0.6\ R_E \quad (10) \\ 2\times10^{-6} - 1.5\times10^{-6}\cdot Y^2 \quad s^{-1} & , \quad X > 0.6\ R_E \text{ and } |Y| \le 0.8\ R_E \quad (11) \\ 10^{-6} \quad s^{-1} & , \quad X > 0.6\ R_E \text{ and } 0.8\ R_E < |Y| < 1\ R_E \quad (12) \end{cases}$$

Equation 10 models the downstream reduction in ionization frequency within Europa's atmosphere. We apply it within 0.15 R_E (~2 H_{O_2}) of Europa's surface as the plasma flows past the moon. The flux tubes moving around the flanks of Europa travel through a larger portion of the atmosphere and are cooled faster compared to the tubes that travel above the poles. Therefore, the ionization frequency in the center of the wake $\left(\nu_{ei,0} = 2\times10^{-6}\ s^{-1}\right)$ is larger than in its flanks $\left(\nu_{ei,0} = 10^{-6}\ s^{-1}\right)$. We prescribe the decrease in ionization frequency in the wake with Equations 11 (center) and 12 (flanks). Figure 2b shows the spatial distribution of such a non-uniform ionization frequency in the equatorial plane. It is worth noting that this non-uniform description of the ionization frequency is not implemented in a self-consistent manner in the code, that is, the spatial distribution is prescribed at the beginning of the simulation and is not updated throughout it. This would require a self-consistent calculation of the electron temperature which is beyond the scope of our current MHD model.

2.4.2. Electron Beams Ionization Frequency

We include in our study the recently detected electron beams at Europa following the concept of "sheets of beamed electrons" introduced by Allegrini et al. (2024a). In this description, as the electrons travel along the magnetic field lines, they are also advected downstream of the moon, which results in so-called sheets of beamed electrons. In other words, the sheets are the two-dimensional manifold described by the plasma velocity streamlines and the background magnetic field lines. The electron beams interact with Europa's atmosphere and ionize the neutral gas along their path. We incorporate this effect in our model by including sheets of enhanced electron impact ionization frequency along the velocity streamlines that correspond to the observed location of the beams.

As pointed out by Allegrini et al. (2024a), the electron beams are present within a region slightly smaller than Europa's geometric wake, flanked by the two strongest beams at 09:34:25 (Beam 1) and 09:36:15 UTC (Beam 2). The beams are visible as enhanced electron fluxes parallel and anti-parallel to the direction of the magnetic field in the energy and pitch angle spectrograms (panels (a) and (b) in Figure 3, respectively) obtained from the JADE electron measurements (Allegrini et al., 2024a). Coincident with both beams, sudden jumps in the magnetic field (panels (c) to (e)) are observed in the magnetometer data, especially in the B_x component, as highlighted by the blue and red arrows in the bottom of Figure 3. Between these two largest electron beams, several beams of smaller amplitude also occurred. We include them as a series of eight consecutive beams (labeled 3.*i*, where *i* denotes the *i*-th beam in the series) separated by 10-s intervals, with the first beam at 09:34:50 UTC and the last one at 09:36:00 UTC, as indicated by the horizontal green arrow in Figure 3. The second column of Table 1 shows the time of occurrence of each beam in our model. In addition, panel (f) displays the electron impact ionization rate of O_2 along the trajectory of Juno inferred from JADE electron measurements (Szalay et al., 2024) and averaged over 10 s intervals. Enhanced values of the ionization frequency coincide in time with the occurrence of the two largest beams and with the sudden perturbations in the magnetic field.

In this work, we build upon the results of Allegrini et al. (2024a) and Szalay et al. (2024), and we investigate to what extent the electron beams, which locally enhance the electron impact ionization frequency, contribute to the observed perturbations in the magnetic field and the plasma density. For this purpose, we implement the sheets of beamed electrons in our MHD model with the following procedure:

1. We take the EPhiO (X, Y, Z) coordinates of the occurrence of Beams 1 and 2 and the series of beams 3.*i* along Juno's trajectory as seed points (third column in Table 1). These are highlighted in green for Beams 1 and 2 in the 3D visualizations of Figure 4. For the sake of clarity, we only show the seed points of these two beams.
2. From each seed point, we calculate a velocity streamline using a Runge-Kutta 4th order method. We trace the streamlines both in backward (i.e., toward Europa) and forward direction (i.e., downstream into the wake), and we use an iteration length of 0.05 R_E. The resultant streamlines traced from the seed points of Beams 1 and 2 are indicated in blue in Figure 4.

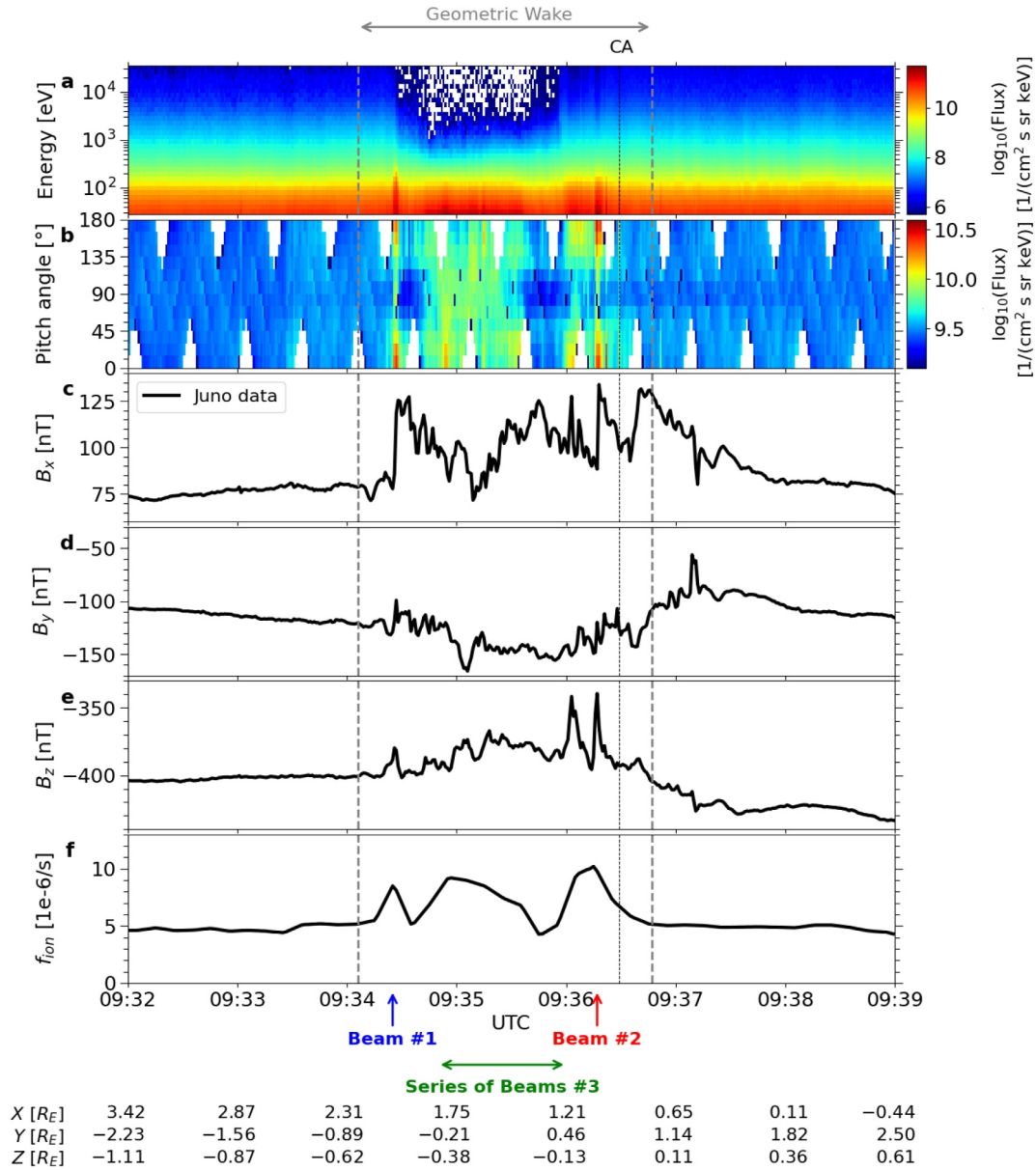

Figure 3. Juno electron fluxes and magnetic field data along the flyby trajectory: (a–b) electron intensity and pitch angle spectrograms measured by the Jovian Auroral Distributions Experiment (JADE) detector (Allegrini et al., 2024a), (c–e) magnetic field components recorded by the magnetometer, and (f) electron impact ionization frequency of O_2 derived from JADE electron observations (Szalay et al., 2024). The dashed black line labeled closest approach (CA) displays the CA of Juno, and the area limited by the dashed gray lines indicates the passage of the spacecraft through the geometric wake. The time occurrence of the beams throughout Europa's wake is indicated by arrows.

3. All points on each velocity streamline are then seed points for magnetic field lines, also traced using a Runge-Kutta 4th order method. We show a few of these magnetic field lines in gray in both panels of Figure 4.
4. The coordinates of all the magnetic field lines along each velocity streamline represent a sheet of beamed electrons, colored in red in Figure 4 for Beams 1 and 2. In total we trace 10 sheets. The extent of the sheets is unconstrained as its detection is limited by the trajectory along Juno's flyby. We arbitrarily extend them 4 R_E into the wake and along the magnetic field lines, as the beams do not play a role where the atmospheric O_2 density vanishes. We extend the sheets of beamed electrons in the upstream direction until the starting point of the streamline intersects with the surface of Europa. Future flybys will provide further characterization of the structure of the beams. The spacing between the seed points from which we trace the sheet corresponding to

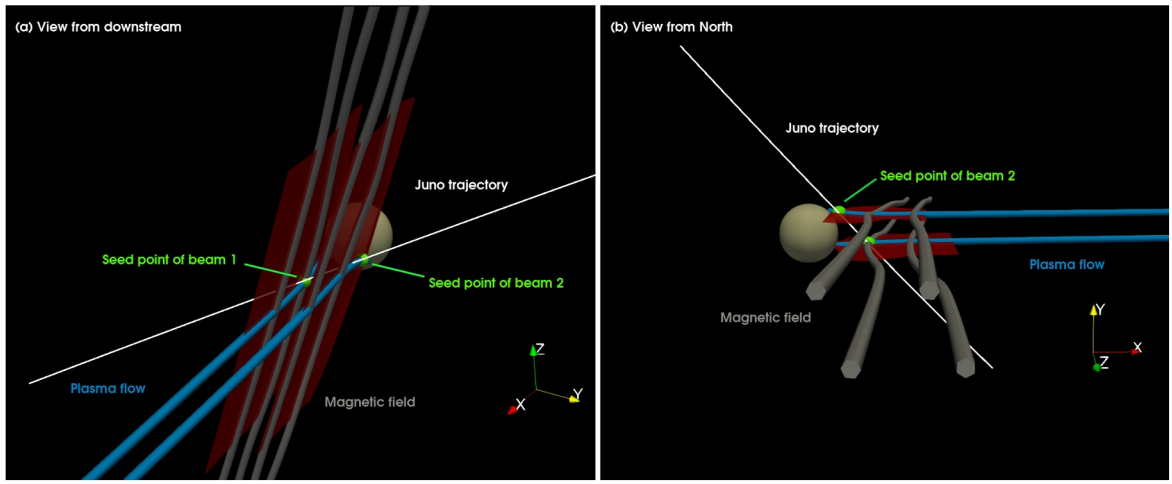

Figure 4. Visualization of the sheets of beamed electrons: (a) from downstream and (b) from North above Europa. See steps (1) to (4) in Section 2.4.2 for further information.

Beam 1 (in the anti-Jovian flank of the wake) and the sheet corresponding to Beam 3.1 (the first in the series of eight consecutive beams throughout the wake) is $\sim 0.38\ R_E$. The seed points of the series of Beams 3.2, 3.3, …, 3.8 are separated each by $\sim 0.15\ R_E$. The spacing between the seed points corresponding to the sheet of Beam 3.8 (the last in the series of beams throughout the wake) and the sheet of Beam 2 (in the sub-Jovian flank of the wake) is $\sim 0.23\ R_E$.

5. We calculate the ionization frequency at the seed point of the j-th sheet, that is, $\nu_{\text{ei,beam}_j,\text{seed point}}$, with $j = \{1, 2, 3.1, 3.2, \ldots, 3.8\}$, by subtracting the non-uniform background ionization frequency (Section 2.4.1) from the ionization frequency from Szalay et al. (2024) at the location of the seed point of the j-th sheet. The values of $\nu_{\text{ei,beam}_j,\text{seed point}}$ for each sheet are shown in the fourth column of Table 1. Furthermore, we take into account the following:
   1. Downstream of the seed points of our sheets, that is, downstream of the location where Juno detected the electron beams, we keep the ionization frequency constant along the streamlines and equal to the value at the seed point, thus $\nu_{\text{ei,beam}_j,\text{streamline}} = \nu_{\text{ei,beam}_j,\text{seed point}}$. This assumption does not affect our MHD simulations, since we aim to model the magnetic field and plasma density along the trajectory of Juno, and it is only the ionization upstream of the trajectory that has an impact on the observed magnetic field and plasma perturbations. This scenario is presented in yellow in Figure 5, for the particular case of Beam 1.
   2. Upstream of the seed points, we consider two possibilities:
      a. In the first scenario, we keep the ionization frequency constant along the streamlines with the same value as at the seed point, thus $\nu_{\text{ei,beam}_j,\text{streamline}} = \nu_{\text{ei,beam}_j,\text{seed point}}$, similar to step 5.1.

Table 1
Parameters of Sheets of Beamed Electrons in the MHD Model

Electron beam number	Time (UTC)	Seed point (X, Y, Z) (R_E)	$\nu_{\text{ei, beam, seed point}}$ $(\times 10^{-6}\ \text{s}^{-1})$	β	w (R_E)
1	09:34:25	(2.1, −0.6, −0.51)	7.06	4.5	0.1
2	09:36:15	(1.07, 0.63, −0.07)	8.82	2	0.1
3.1	09:34:50	(1.86, −0.32, −0.41)	6.06	2.5	0.06
3.2	09:35:00	(1.77, −0.21, −0.37)	7.17	2.5	0.06
3.3	09:35:10	(1.68, −0.09, −0.33)	6.81	3.5	0.06
3.4	09:35:20	(1.58, 0.02, −0.29)	6	3.5	0.06
3.5	09:35:30	(1.49, 0.13, −0.25)	5.13	5.5	0.06
3.6	09:35:40	(1.39, 0.24, −0.21)	2.69	10	0.06
3.7	09:35:50	(1.3, 0.35, −0.17)	1.99	9.5	0.06
3.8	09:36:00	(1.21, 0.46, −0.13)	4.44	4	0.06

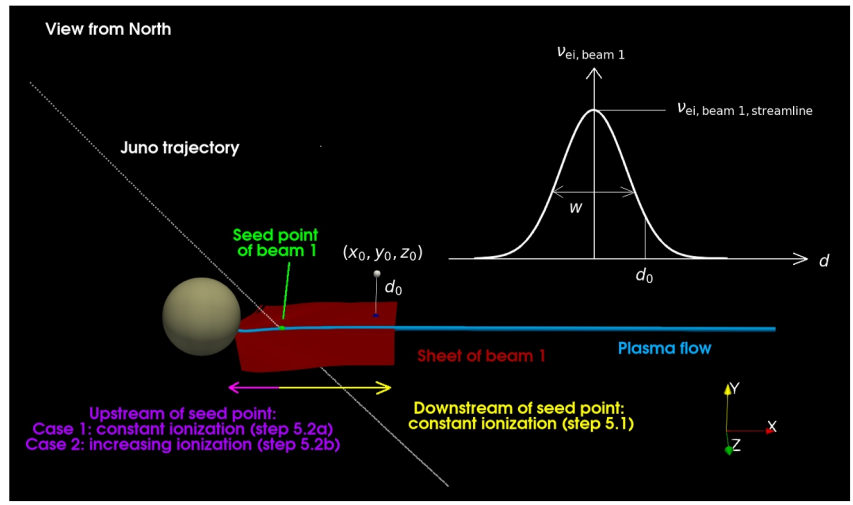

Figure 5. Schematic visualization of the calculation of the enhanced electron impact ionization frequency due to Beam 1 at an arbitrary point with coordinates (x_0, y_0, z_0) separated a distance d_0 from the sheet corresponding to Beam 1. See steps (5) to (7) in Section 2.4.2 for a detailed description.

b. In the second scenario, we assume that the ionization frequency increases with distance from the seed point. The rationale behind this assumption is similar to the non-uniform background ionization frequency (Section 2.4.1): as the electron beams interact with Europa's atmosphere and are advected downstream, they are cooled down and the ionization frequency decreases. Therefore, it might be the case that the electron impact ionization rates upstream of the seed points are larger than the actual values derived along the trajectory of Juno. We return to this hypothesis in Section 3.3, where we compare the spacecraft observations and the results from our MHD model, as possible evidence to support this statement. In order to account for such an upstream increase, we add to the ionization frequency at the seed point a factor that depends on the distance from the seed point along the streamline ($d_{\text{seed point}_j}$) and a coefficient β_j. For sake of simplicity, we assume that the distance along the streamline is only a function of the X coordinate, that is, $d_{\text{seed point}_j} = X_{\text{seed point}_j} - X_{\text{along streamline}}$. The factor β_j controls the upstream increase of the ionization frequency, and we determine its values (Table 1, fifth column) by finding the best fit (by eye) between our MHD simulations and the observed magnetic field and plasma density (Section 3.3). The upstream ionization frequency is given by:

$$\nu_{\text{ei,beam}_j,\text{streamline}} = \left(d_{\text{seed point}_j} \cdot \frac{\nu_{\text{ei,beam}_j,\text{seed point}} \cdot (\beta_j - 1)}{X_{\text{seed point}_j} - X_{\text{streamline}_{0,j}}} \right) + \nu_{\text{ei,beam}_j,\text{seed point}}, \tag{13}$$

where $X_{\text{streamline}_{0,j}}$ is the starting point of the streamline of the j-th sheet. In our case, the starting points of all the streamlines lie on Europa's surface, and thus there are no sheets of beamed electrons when the field lines intersect with Europa. Both scenarios (a) and (b) are shown in magenta in Figure 5.

6. We compute the minimum distance d_j from each cell of our computational domain to the j-th sheet. We schematically show this step for an arbitrary point with coordinates (x_0, y_0, z_0) in Figure 5.
7. We calculate the enhanced electron impact ionization frequency $\nu_{\text{ei, beam}_j}$ in each cell due to the j-th electron beam using a Gaussian of width w_j:

$$\nu_{\text{ei,beam}_j} = \nu_{\text{ei,beam}_j,\text{streamline}} \cdot \exp\left[-\left(\frac{d_j}{w_j} \right)^2 \right] \tag{14}$$

we explore different possible values for the width w of the Gaussians. We find that a width of 0.1 R_E for Beams 1 and 2, and a width of 0.06 R_E for each of the Beams 3.i in the wake yields the closest match between our prescribed total electron impact ionization frequency along the flyby trajectory and the profile of ionization rate of O_2 from Szalay et al. (2024). We also take into consideration the fit between our modeled magnetic field and plasma density and the data by Juno when constraining the values for w_j. We come back to this point later in Section 3.3. The sketch in the upper right corner of Figure 5 illustrates this step for the point with coordinates (x_0, y_0, z_0) separated a distance d_0 from the sheet corresponding to Beam 1.

8. The total enhanced electron impact ionization frequency in each cell due to the combined effect of all the electron beams $\nu_{\text{ei, beams}}$ is given by the sum:

$$\nu_{\text{ei, beams}} = \sum_j \nu_{\text{ei, beam}_j}. \tag{15}$$

We display the total electron impact ionization frequency in the equatorial plane due to the electron beams in Figures 2c and 2d. In both panels the ionization frequency is clearly enhanced downstream of Europa at the streamlines from which we trace the sheets of beamed electrons. Panel (c) corresponds to the first case of step (5.2), where the ionization frequency upstream of the seed point does not increase, while panel (d) shows the results from the second case of step (5.2), where the upstream enhancement of ionization frequency with respect to the each of the seed points is visible.

The total electron impact ionization frequency ν_{ei} in each cell of our domain is given by the sum of the background ionization and the enhanced ionization due to the electron beams:

$$\nu_{\text{ei}} = \nu_{\text{ei},0} + \nu_{\text{ei, beams}}. \tag{16}$$

In Figures 2e and 2f we present the distribution of the total electron impact ionization frequency ν_{ei} in the equatorial plane. In both cases we consider a non-uniform background ionization ($\nu_{\text{ei},0}$ from panel (b)). In Figure 2e we assume that the ionization due to the beams does not increase in the upstream direction ($\nu_{\text{ei, beams}}$ as in panel (c)), whereas in Figure 2f we enhance it following the procedure outlined above ($\nu_{\text{ei, beams}}$ as in panel (d)).

We must emphasize that our implementation of the enhanced ionization due to the electron beams is carried out in a not self-consistent way, similar to the scenario of the non-uniform background ionization frequency (Section 2.4.1). First, we perform a simulation that does not include the sheets of beamed electrons. We use the results of this run to trace the velocity streamlines and to build the two-dimensional sheets. Then, in order to account for the effect of the electron beams, we start a new model run, and we apply the previously traced sheets to calculate the enhanced ionization frequency $\nu_{\text{ei, beams}}$ (Equation 15) and the total electron impact ionization frequency ν_{ei} (Equation 16). We store the corresponding values in a 3D grid and proceed with the MHD simulation, keeping the ionization frequency unchanged throughout the model run.

2.5. Induction in a Subsurface Water Ocean

Jupiter's magnetic moment is tilted by $\sim 10°$ with respect to its spin axis, and therefore, the x and y components of the background magnetic field vary periodically at Europa's location. This results in an inducing field with the ~11.1 hr synodic rotation period of Jupiter in the rest frame of Europa. The time-varying inducing background magnetic field is included in our model with the following equations from Schilling et al. (2007):

$$B_{0,x}(\lambda_{\text{III}}) = -84 \text{ nT } \sin(\lambda_{\text{III}} - 200°), \tag{17}$$

$$B_{0,y}(\lambda_{\text{III}}) = -210 \text{ nT } \cos(\lambda_{\text{III}} - 200°). \tag{18}$$

with System III longitude λ_{III}. The time-varying inducing background field drives electric currents in Europa's subsurface water ocean, and thus creates a time-varying induced magnetic dipole field (Khurana et al., 1998; Saur et al., 2010). Considering a spatially homogeneous external time-varying inducing field and a radially symmetric ocean, the resultant induced field is dependent on the conductivity, the thickness, and the depth of the ocean. Similar to Blöcker et al. (2016) and Cervantes and Saur (2022), we assume an ocean that is 100 km thick and lies

25 km below the surface, with a conductivity of $\sigma = 3$ S m^{-1}. This results in an induced field with amplitude $A = 0.96$ and phase $\Phi = -4.3°$. The inner boundary conditions at the surface of Europa (Section 2.6) account for the time-variable induced field within the subsurface ocean.

2.6. Numerics and Boundary Conditions

In order to solve the set of MHD differential Equations 1–4, and to self-consistently calculate the magnetic field and bulk plasma properties, we use a modified version of the freely distributed PLUTO code, widely applied in computational astrophysics. Mignone et al. (2007) presents a detailed description of the algorithms used in PLUTO. In particular, the code has already been successfully employed in the context of moon-magnetosphere interactions by Duling et al. (2022) in order to model Ganymede's plasma interaction during the Juno flyby on 7 June 2021.

At the inner boundary, that is, Europa's icy surface, plasma is assumed to be absorbed, and we apply open boundary conditions for the four MHD variables. In addition, we constrain the radial component of the plasma bulk velocity so that $v_r \leq 0$. The insulating nature of the moon's surface also inhibits any electric currents to penetrate it. Duling et al. (2014) derived boundary conditions for the magnetic field, ensuring there is no radial electric current. The boundary condition also accounts for any internal potential fields from below the surface, for example, caused by induction in an ocean below the non-conducting icy crust. Finally, at the outer upstream boundary we apply inflowing conditions with values equal to the upstream conditions and at the outer downstream side we employ open boundary conditions.

3. MHD Simulations of Europa's Plasma Interaction

We now quantitatively investigate Europa's plasma interaction and the influence of the electron beams on the magnetic field environment for the conditions of the Juno flyby by means of the MHD model, as described in Section 2. We also compare our simulations results with: (a) the magnetic field measurements collected by the magnetometer, (b) the electron impact ionization frequency of O_2, and (c) the total ion number density, the latter two derived from JADE plasma observations.

The first four panels of Figure 6 show in black the magnetometer data for the flyby. As mentioned in Section 2.4.2, sudden jumps in the B_x component with amplitudes of ∼50 and ∼40 nT are observed coinciding with the occurrence of Beams 1 and 2, respectively. Between both peaks, and throughout the passage of Juno across the geometric wake, B_x exhibits subsequent dips and enhancements, which we ascribe to the series of Beams 3. The B_y and B_z components also show fluctuations as the spacecraft traverses the wake and exits it, albeit of smaller amplitude. A double-spike perturbation in B_z, and to some extent in B_x, is apparent shortly before the time of CA, with the second spike at the location of Beam 2. As mentioned in Section 1, the modeling study by Addison et al. (2024) ascribes the broad B_x enhancement around ∼09:34:30 UTC to a deviation of the magnetospheric upstream plasma flow from the corotational directional towards the sub-Jovian hemisphere. We do not include this tilt in the plasma flow in our MHD model, and instead, we propose that the electron beam at this location (i.e., Beam 1) contributes to the sudden jump in B_x.

We display plasma data from the Europa flyby (Szalay et al., 2024) in the bottom two panels of Figure 6. The electron impact ionization frequency along Juno's trajectory peaks at 8.5×10^{-6} s^{-1} and 10.2×10^{-6} s^{-1} in the first and the second beams, respectively. In the region between both largest beams, that is, throughout our series of beams number 3, the maximum ionization frequency reaches a maximum of 9.2×10^{-6} s^{-1}. The plasma observations from JADE reveal a gradual twofold increase in the total ion number density from an upstream value of ∼100 cm^{-3}, reaching its maximum ∼30 s prior to CA, inside Europa's geometric wake. This twofold increase is analogous to the peak electron density of ∼330 cm^{-3} near Europa while the surrounding magnetospheric density is within the range of 50 to 150 cm^{-3} (Kurth et al., 2023).

In this study, we aim to answer if: (a) the sudden, rapid perturbations in the magnetic field timeseries, mainly evident in the B_x component, from ∼09:34 until ∼09:37 UTC, and (b) the wake full of ionized plasma downstream of Europa, are imposed by the presence of electron beams at the locations mentioned in Section 2.4.2. In order to test these hypotheses, we carry out over 500 model runs, and we systematically vary: (a) the O_2 atmospheric distribution around the moon, (b) the background ionization frequency, and (c) the parameters of the sheets of

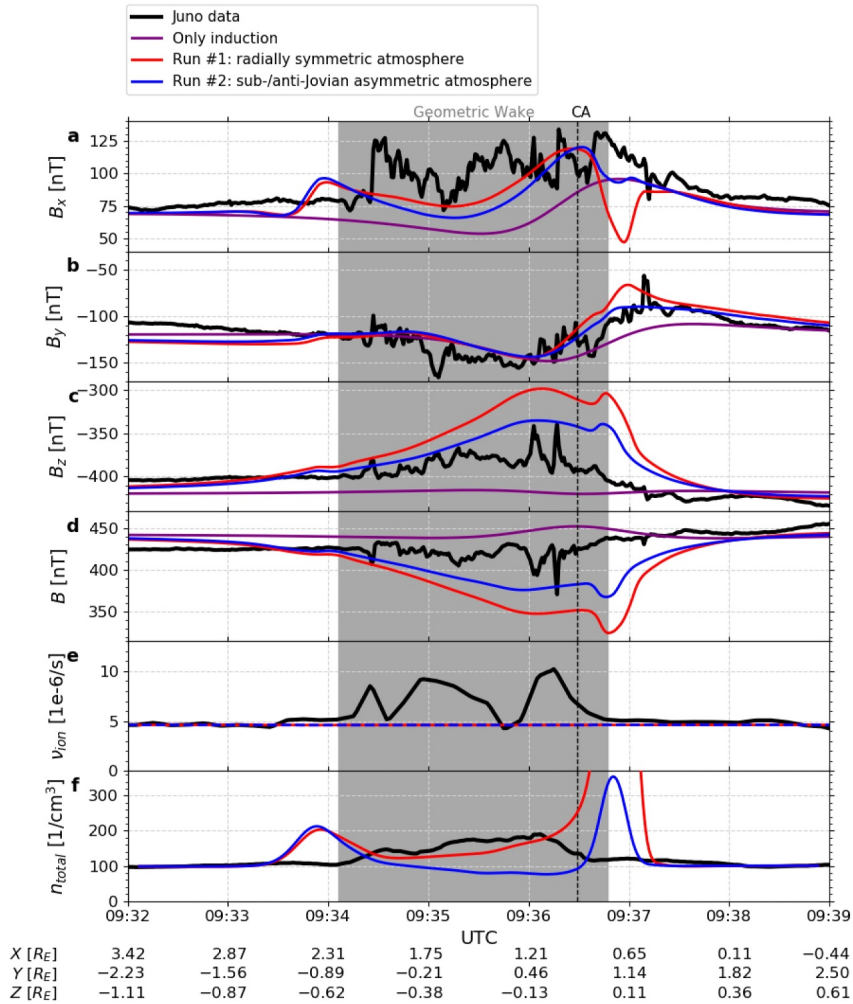

Figure 6. Comparison between Juno measurements (black) and magnetohydrodynamic (MHD) results for two models of Europa's atmosphere: runs 1 (radially symmetric) and 2 (sub-/anti-Jovian asymmetric) in red and blue, respectively: (a–c) magnetic field components (a–c), (d) total field magnitude, (e) electron impact ionization frequency of O_2, and (f) total ion number density. The superposition of the Jovian background field and Europa's induced dipole (i.e., no plasma interaction) is shown in purple in panels (a–d). The dashed black line labeled closest approach (CA) displays the CA of Juno, and the shaded gray area indicates the passage of the spacecraft through the geometric wake. See Table 2 for further information on the MHD runs.

beamed electrons (location of the seed points, width of the Gaussian distributions, and upstream increase of ionization frequency). Here, we present the results of five of these runs, the details of which are shown in Table 2.

In the next three subsections we focus on the effect of each of the above-mentioned parameters on Europa's plasma interaction, by varying them one at a time between subsequent simulations. In Section 3.1 we concentrate

Table 2
Summary of MHD Runs

Run	O_2 atmosphere	Background ionization frequency	Electron beams
1	Radially symmetric	Uniform	No
2	Sub-/anti-Jovian asymmetric	Uniform	No
3	Sub-/anti-Jovian asymmetric	Non-uniform	No
4	Sub-/anti-Jovian asymmetric	Non-uniform	Yes
5	Sub-/anti-Jovian asymmetric	Non-uniform	Yes, with upstream increase in ionization frequency

on the distribution of O_2 around the moon and present the results of Runs 1 (radially symmetric atmosphere) and 2 (sub-/anti-Jovian asymmetric atmosphere); and then, in Section 3.2 we look in detail into the background ionization frequency and show the results of Runs 2 (asymmetric atmosphere + uniform ionization) and 3 (asymmetric atmosphere + non-uniform ionization). Finally, in Section 3.3 we examine the role of the electron beams on the plasma interaction and focus on the results of our MHD Runs 3 (asymmetric atmosphere + non-uniform ionization), 4 (asymmetric atmosphere + non-uniform ionization + beams), and 5 (asymmetric atmosphere + non-uniform ionization + beams with upstream increase in ionization).

3.1. Effects of an Asymmetric Atmosphere

We start by assuming a radially symmetric atmosphere (Equation 8) and a uniform background ionization frequency $\left(\nu_{ei,0} = 4.6 \times 10^{-6}\ s^{-1}\right)$, a standard description frequently applied in MHD simulations of Europa's plasma interaction. In this setup (Run 1: radially symmetric), we do not account for the presence of electron beams. The results are presented in red in Figure 6. First of all, the modeled B_x component differs significantly from the measurements by Juno. The enhancement shortly after entering the wake occurs ∼40 s earlier than observed, and its amplitude is roughly half of the measured value. Also, none of the dips and enhancements in the wake are reproduced with this run. Moreover, it is particularly relevant to note the large decrease by ∼70 nT between CA and ∼09:37:00 UTC. Such a pattern is not observed in the magnetometer data. We will further discuss this striking feature in the next paragraph. The observed B_y perturbations are largely well reproduced with this setup, except shortly after Juno exits the wake. In contrast, the B_z component is in general overestimated with this model by ∼50–100 nT. Since we assume a uniform background ionization and we neglect the enhanced ionization due to the beams in this run, the total electron impact ionization frequency is constant and equal to its upstream value of $4.6 \times 10^{-6}\ s^{-1}$. Finally, the total ion number density is overestimated at the same locations where the modeled B_x is perturbed: shortly before entering the wake, and especially, after exiting it. Downstream in the wake, the modeled number density increases, on average, 50% with respect to its upstream value of 100 cm^{-3}. Analogous to the JADE ion densities reported by Szalay et al. (2024), we also smooth the total number density with a 30 s sliding boxcar. We calculate the residuals for the magnetic field components, the total field magnitude, and the total ion number density as the difference between the measurements provided by Juno and our model predictions, and we plot them along the flyby trajectory in Figure S1 in Supporting Information S1.

We return our attention to the above-mentioned lack of agreement between the modeled (Run 1) and the observed B_x perturbations after CA. For this purpose, we show in purple in Figures 6a–6d the sum of the Jovian background magnetic field $\mathbf{B}_0$ and Europa's induced dipole (i.e., we neglect the effects due to plasma interaction). The B_y component is in general well reproduced with this superposition. However, the negative ΔB_x signature from the "induction only" case does not correspond to the observed positive ΔB_x perturbation before ∼09:36:15 UTC. On the other hand, after the time of CA, Europa's induced field can explain the positive ΔB_x, in line with the measured magnetic field, in stark contrast to the negative ΔB_x perturbation predicted by the MHD model.

Based on the pattern of the ΔB_x perturbations on the trajectory of Juno, and in order to reproduce the magnetic field measured by the spacecraft, we propose the following scenario: the inbound segment of the flyby is "plasma interaction-dominated", whereas the outbound portion (roughly after CA) is "induction-dominated." We hypothesize that one way to gradually reduce the effects of the plasma interaction is by considering an asymmetric distribution of O_2, the column density of which decreases as Juno travels towards Jupiter, from the anti-Jovian to the sub-Jovian hemisphere of Europa. This argument explains our choice for the asymmetric atmosphere given by Equation 9.

Our next model run (number 2: sub-/anti-Jovian asymmetric) accounts for such an asymmetry, while the rest of the parameters unchanged with respect to Run 1. The results are presented in Figure 6 in blue. The modeled B_x shows the effects of the plasma interaction dominating before CA, and after it, the main contribution to the measurements stemming from the induced field. We interpret the presence of such an induction signal as evidence of the presence of Europa's subsurface water ocean. Furthermore, the agreement with the observed B_z component improves, although the model still overestimates the data, by ∼50 nT on average along the flyby trajectory. The total ion number density decreases as Juno traverses Europa's wake towards Jupiter, similar to our asymmetric atmosphere model, but opposite to the gradual increase in the plasma data. With such an asymmetric atmosphere, the wake is nearly empty of plasma.

Zimmer et al. (2000) provides a range of values for the amplitude A of the induced field between 0.7 and 1. As mentioned in Section 2.5, for our assumptions of Europa's ocean, $A = 0.96$. Smaller values of the amplitude, towards the lower limit of 0.7, would smooth the sub-Jovian/anti-Jovian asymmetry and reduce the contribution of the induced field in the outbound portion of the flyby by ∼10 nT. Nevertheless, values for A much larger than 0.7 (i.e., induced magnetic field almost saturated), and similar to the amplitude of the induced field in our study, have also been reported in the literature (e.g., Schilling et al., 2004; Schilling et al., 2008).

3.2. Effects of a Non-Uniform Distribution of the Background Electron Impact Ionization

Our results from Run 2 show that introducing an asymmetric atmosphere in our MHD model improves the fit to the observed B_x component, particularly after the time of CA. On the other hand, such an asymmetry did not reduce the overestimation in B_z, especially in the segment of the flyby after ∼09:35:00 UTC. Taking into account the fact that perturbations in B_z are driven by compressional waves, one possible way to match the observed B_z is to further decrease the atmospheric density in Europa's sub-Jovian hemisphere. However, we do not consider this scenario plausible, since the neutral O_2 in Europa's atmosphere accumulates approximately uniformly over the moon (Bagenal & Dols, 2020; McGrath et al., 2004; Plainaki et al., 2018), and thus, such a strong density gradient is not likely to develop around Europa. Moreover, the column densities in our asymmetric model (5×10^{17} to 10^{18} m^{-2}) are in the lower limit of the measured O_2 abundances at Europa (Roth, 2021), and column densities even lower than these values have not been observed.

In addition to the neutral O_2 number density, the source term Pm_n on the right hand side of the continuity Equation 1 is also controlled by the ionization frequency ν_{ion}. If the ionization frequency decreases, the production of plasma and the total plasma mass density ρ are also reduced, and in turn, the amplitudes of the perturbations of the B_z component diminish as well. Therefore, we introduce a more realistic, non-uniform distribution of the electron impact ionization frequency, driven by the reduction of electron temperature in Europa's atmosphere and in its wake, as physically expected and modeled by Saur et al. (1998). This more realistic description leads to a decrease of the ionization frequency in the wake downstream of the moon below its upstream value of $\nu_{\text{ei},0} = 4.6 \times 10^{-6}$ s^{-1}, as presented in Section 2.4 and in Figure 2b.

We account for such a non-uniform background ionization frequency in our Run 3 (asymmetric atmosphere + non-uniform ionization), and we keep the remainder of the setup of the MHD model the same as in Run 2. Figure 7 shows the results from Runs 2 and 3 in blue and green, respectively. The amplitudes of our modeled B_x and B_z components from Run 3 are now decreased along Juno's passage throughout the wake, with respect to Run 2. However, the sharp jump around ∼09:34:30 UTC, mostly prominent in B_x, is still not reproduced by our Run 3.

The electron impact ionization frequency along the flyby drops to $\nu_{\text{ei},0} = 10^{-6}$ s^{-1} as Juno enters and exits the wake around ∼09:34:00 and ∼09:37:00 UTC, respectively, and it reaches a local maximum of $\nu_{\text{ei},0} = 2 \times 10^{-6}$ s^{-1} at ∼09:35:20 UTC. As a consequence of the reduced ionization frequency downstream of Europa, the total ion number density also decreases and the wake is relatively devoid of plasma, especially in the second half of the flyby, in contrast to the plasma density measurements from JADE. We provide the residuals along the flyby trajectory between the spacecraft data and the model predictions of Run 3 in Figure S1 in Supporting Information S1.

3.3. Effects of the Electron Beams in Europa's Wake

As shown in the previous section, our setup of Run 3 yields signatures in the magnetic field (particularly in the B_x component prior to CA) and the total ion number density that are not consistent with the spacecraft data. Furthermore, our prescribed electron impact ionization frequency does not coincide with the profile derived from JADE electron measurements.

In their recent paper, Allegrini et al. (2024a) show that Europa's wake as sampled by Juno during its flyby is filled with electrons, and they suggest that the electron beams might play an essential role in filling the wake with plasma. The authors also state that, in comparison to the background electrons in Europa's environment, the beams ionize several times more atoms and molecules in the moon's atmosphere. Such a locally enhanced ionization would correspond to the peaks in the profile of ionization frequency from Szalay et al. (2024). Moreover, Allegrini et al. (2024a) also discuss that the beams contribute to the perturbations in the magnetic field,

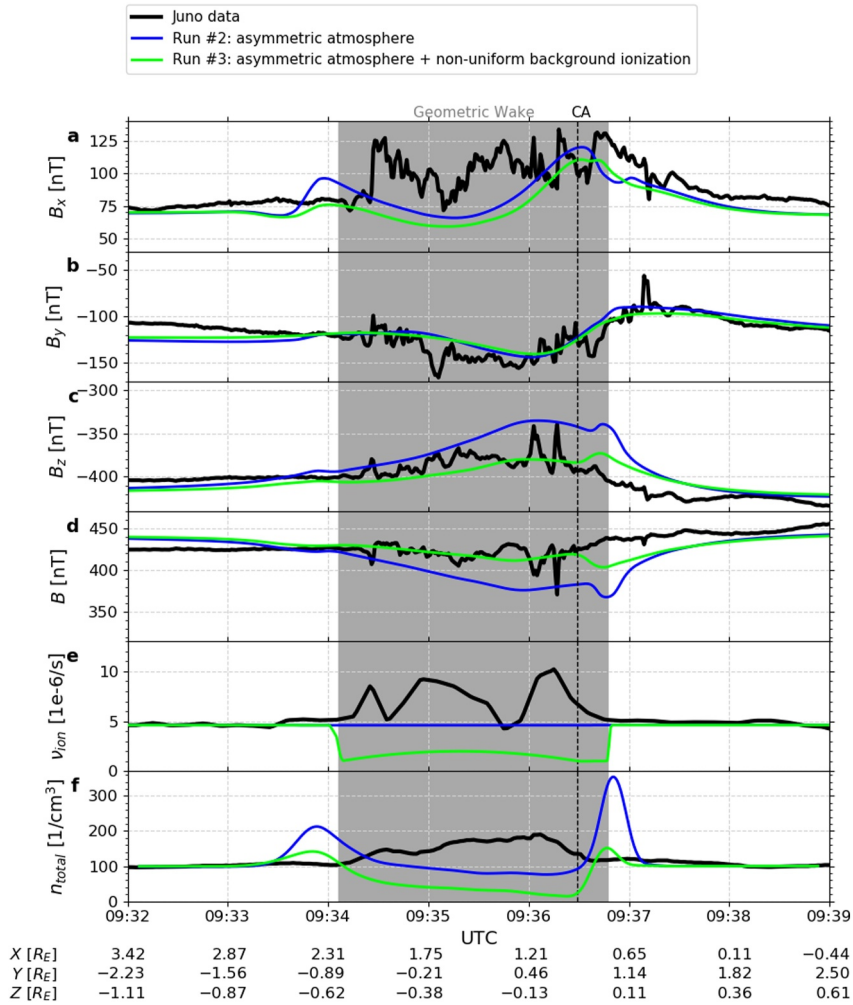

Figure 7. Same as Figure 6, but for magnetohydrodynamic (MHD) results assuming a sub-/anti-Jovian asymmetric atmosphere and two configurations of the background electron impact ionization frequency: runs 2 (uniform background ionization) and 3 (non-uniform background ionization), in blue and green, respectively. See Table 2 for further information on the MHD runs.

especially in B_x. These arguments suggest that the electron beams might be a candidate ingredient to explain the lack of agreement between the observations by Juno and our model results of Runs 1 to 3.

In order to investigate the effect of the electron beams in Europa's environment, we include them in our MHD model following the procedure outlined in Section 2.4.2 and using the parameters from Table 1. This setup corresponds to Runs 4 (asymmetric atmosphere + non-uniform ionization + beams) and 5 (asymmetric atmosphere + non-uniform ionization + beams with upstream increase in ionization). The only difference between both runs is that, in the former (Run 4) we keep the ionization frequencies due to the beams along the streamlines in the upstream direction equal to the corresponding value at the seed point (case (a) in step (5.2) in Section 2.4.2), whereas in the latter (Run 5), we increase them according to Equation 13 and the values of β in Table 1 (case (b) in step (5.2)). The rest of the model parameters are kept unchanged relative to Run 3. As mentioned in Section 2.4.2, we explore several values of the width w for the Gaussians that we apply to model the enhanced ionization due to the beams. Our choice of $w = 0.1\ R_E$ (Beams 1 and 2) and $w = 0.06\ R_E$ (series of Beams 3) provides the best fit to the plasma and magnetic field measurements and also reproduces the overall shape of the ionization frequency profile from Szalay et al. (2024). We consider a larger value of w for Beams 1 and 2 compared to the narrower beams in the wake, since these two were reported to be the strongest beams of all during the flyby (Allegrini et al., 2024a).

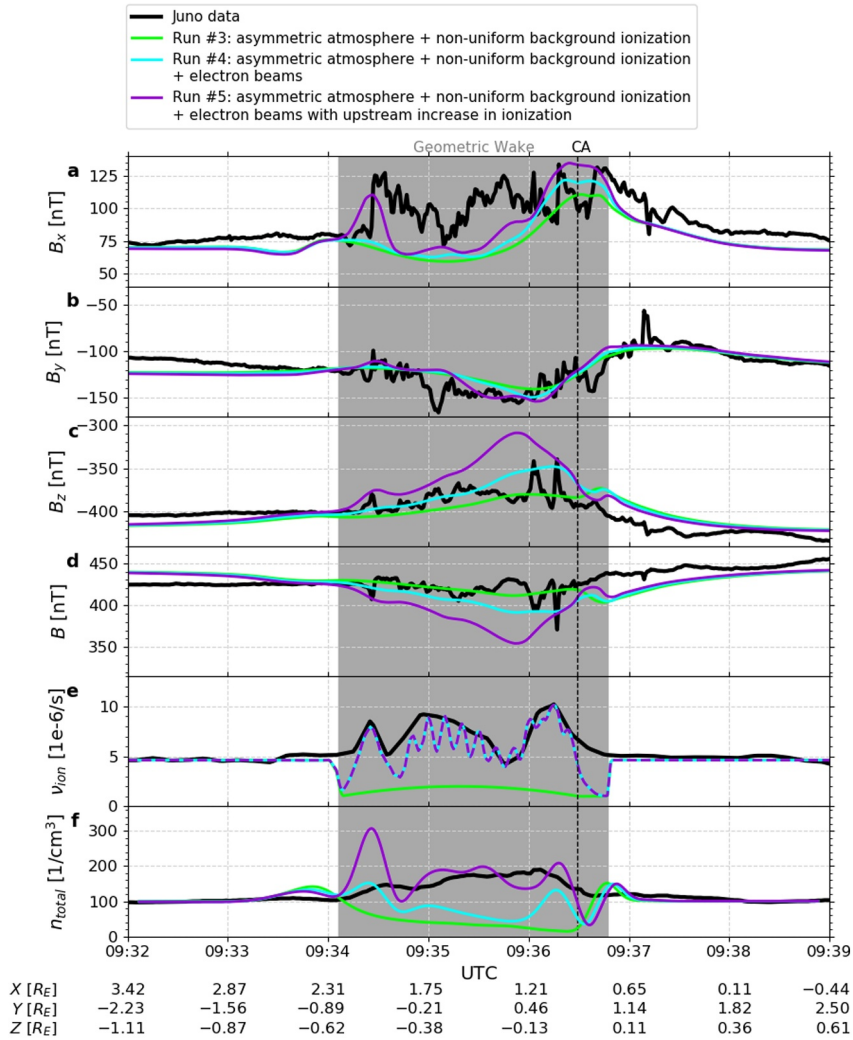

Figure 8. Same as Figure 6, but for magnetohydrodynamic (MHD) results assuming a sub-/anti-Jovian asymmetric atmosphere and a non-uniform background electron impact ionization frequency: runs 3 (without electron beams), 4 (with electron beams), and 5 (with electron beams and upstream increase in ionization) in green, cyan, and purple, respectively. See Table 2 for further information on the MHD runs.

Our results from Runs 4 and 5 are displayed in Figure 8, and we also plot the output from Run 3, in order to clearly contrast the simulations before and after including the electron beams. In addition, Figure S2 in Supporting Information S1 provides the magnetic field and total ion number density residuals along the flyby trajectory for Runs 4 and 5. We first discuss the results of Run 4 (in cyan) in Figure 8. With this setup, the fit to the observed B_z component improves. In contrast, the modeled B_x only marginally increases and the sudden jump at the location of Beam 1, followed by the subsequent dips and enhancements (the series of Beams 3) is not reproduced by this model run. Since our values of the enhanced ionization frequencies due to the beams are based on the rates derived from JADE measurements, the general pattern of the total electron impact ionization frequency coincides with the observed profile along the trajectory of Juno. However, the total ion number density is underestimated with this setup, and the decrease in our modeled number density throughout the wake is contrary to the gradual increase in the plasma data. Two local maxima in density are observed at the location of Beams 1 and 2.

We focus again on the lack of agreement between the observed and modeled (Run 4) B_x component and total ion number density (Figures 8a and 8f). The output of our MHD simulations along the flyby depends on the values *upstream of the trajectory*, however, the profile of electron impact ionization rate of O_2 from Szalay et al. (2024) was derived from measurements *along the trajectory*. Thus it means that the electron beams might have been

more intense upstream of the flyby, that is, the ionization frequency due to the beams $\nu_{ei,\ beams}$ might have been larger upstream than at the locations where Juno detected them. Furthermore, as described in Section 2.4.2, the electron impact ionization frequency decreases as the electron beams collide with neutrals in Europa's atmosphere and are advected downstream, which in addition to the above-mentioned misfit with the Juno data explains why we expect such an upstream increase in ionization frequency.

Our MHD Run 5 accounts for the upstream enhancement in the ionization frequency due to the electron beams, and the output of our model is plotted in purple in Figure 8. Our choice of the rate of upstream increase, that is, the parameter β in Equation 13, is constrained by obtaining the best agreement as possible between the modeled and measured magnetic field and plasma density. The results that we show in Figure 8 correspond to the values of β in Table 1, and they represent our closest fit to the Juno data. First of all, and most notably, the peak in the B_x component around 09:34:30 UTC, which we ascribe to Beam 1, is now reproduced by our MHD model. The dips and enhancements in the observed B_x throughout the wake are also present in our results, although our simulation underestimates these signatures by ∼25–40 nT. However, our simulated B_z component is overestimated towards the center of the wake. Since the enhancement of ionization due to the beams is performed only upstream of the trajectory of Juno, the total ionization frequency along the trajectory does not change with respect to Run 4. Finally, our modeled total ion number density overestimates the measured values shortly after entering the geometric wake, at the location of Beam 1, by a factor of ∼2; while afterward, the values from our MHD simulation are in closer agreement with the plasma data. Our setup of Run 5 shows that the electron beams fill the wake with newly ionized plasma, in line with the findings from Allegrini et al. (2024a).

As expected, the pattern of the simulated total ion number density resembles the profile of ionization frequency along the trajectory. This explains, for instance, the decrease in ion number density around 09:36:00 UTC in Runs 4 and 5, since Beams 3.6 and 3.7 have the lowest ionization frequency of all. Moreover, due to fact that these beams are located in the sub-Jovian hemisphere, where the neutral O_2 density is reduced as imposed by our asymmetric atmosphere model, the only way we find to simultaneously produce magnetic field signatures consistent with B_x and number densities in agreement with the data, but without significantly overestimating B_z, is to use a factor $\beta\ \sim 3$ times larger than at the other beams. Finding the optimal rate of upstream increase for Beam 1 proves the most challenging of all, since larger values of β increase the B_x signature in accordance with the magnetometer data, at the expense of overestimating the ion number density. Conversely, smaller values of β provide a better fit to the ion density, but do not reproduce the sharp peak in B_x. We will return our attention to this surplus of plasma density predicted by our model and to the possible overestimation of the effects of the enhanced ionization on the magnetic field in Section 4. For Beam 2 we require a relatively small value of β, as the simulation without upstream increase (Run 4) already provides a good fit to both the magnetic field and the ion density. This is also in agreement with the second half of the flyby being "induction-dominated", which implies that we do not require such a great increase of the ionization frequency in the upstream direction, in other words, we do not need to further enhance the plasma interaction.

Our MHD simulations show that the ionizing effect of the electron beams generates large variations in the magnetic field, particularly in the B_x component. From Ampere's law, the x component of the magnetic field is related to the z component of the electric current density via $\mu_0 J_z \approx -\partial_y B_x$, where we have neglected the $\partial_x B_y$ term as the beams do not have a noticeable effect on B_y. Panels (a) and (b) of Figure 9 present the measured and modeled B_x component, and the modeled J_z component along the flyby trajectory, respectively, before and after introducing the sheets of enhanced ionization in the MHD code (i.e., the output from Runs 3 and 5, respectively). The plasma interaction scenario without electron beams results in current densities in the z component between 10^{-7} and 5×10^{-7} A m^{-2}. These values are analogous to the current densities predicted by previous modeling studies of Europa's plasma interaction that did not include electron beams, for example, Blöcker et al. (2016) and (Saur et al., 1998), which calculated maximum field aligned current densities of 2×10^{-7} A m^{-2} and 4×10^{-7} A m^{-2}, respectively. In contrast, the current densities in the z component from the scenario that accounts for electron beams with upstream increase in the ionization frequency are approximately an order of magnitude larger, and range between 1.6×10^{-6} A m^{-2} and 1.9×10^{-6} A m^{-2} at the locations of Beams 2 and 1, respectively. Allegrini et al. (2024a) employed the above-mentioned simplified form of Ampere's law and the B_x component measured by Juno, and estimated a similar current density of 2×10^{-6} A m^{-2} at the location of Beam 1. These numbers however can only be indirectly compared. Allegrini et al. (2024a) estimated a possible net electric current within the beams. In our simulations the beams themselves do not carry electric current, but act

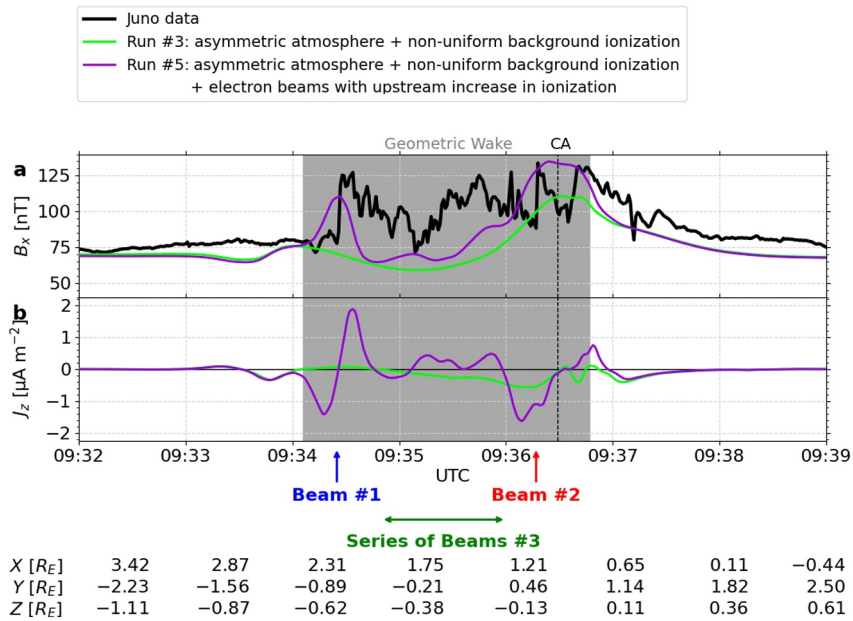

Figure 9. Comparison between Juno measurements (black) and magnetohydrodynamic (MHD) results for two models of Europa's plasma interaction which account for an asymmetric atmosphere and a non-uniform background ionization frequency: runs 3 (without electron beams) and 5 (with electron beams and upstream increase in ionization) in green and purple, respectively. Panel (a) shows the measured and modeled B_x component of the magnetic field, and panel (b) the modeled J_z component of the electric current density. See Table 2 for further information on the MHD runs.

as a locally strongly ionizing medium. This generates resultant magnetic field perturbations and Alfvén winglets which carry bi-directionally distributed, but zero-net electric currents as displayed in Figure 9. This point is discussed further in Section 4.

In order to elucidate the influence of the electron beams on the magnetic field and plasma flow, we perform two additional simpler MHD simulations. We consider a basic geometry such that the background magnetic field points in the negative z direction, that is, $\mathbf{B}_0 = (0, 0, -420)$ nT. The remainder of the upstream plasma parameters v_0, ρ_0, and p_0 are kept unchanged with respect to model Runs 1 to 5, and their values are as specified in Section 2.1. We assume a radially symmetric atmosphere and a uniform background ionization frequency, and we neglect induction in the subsurface water ocean, as these processes would generate additional asymmetries in the plasma interaction, and we are interested in understanding the effect of the electron beams on the magnetic field and plasma environment. In the first simulation we do not account for the presence electron beams in Europa's wake, whereas in the second run we include them. For purposes of clarity, we only consider Beams 1 and 2 in this simplified setup.

We display a 3D visualization of the B_x component for both scenarios in Figures 10a and 10b, before and after including the electron beams, respectively. Panel (a) shows the development of Alfvén wings as regions of perturbed B_x north and south of Europa in the xz plane (Neubauer, 1980). The wings are bent back by a constant angle of $\Theta_A \sim 25°$ relative to the unperturbed background magnetic field. The magnetic field is perturbed in the negative (positive) x direction north (south) of Europa. In contrast, panel (b) reveals the formation of additional Alfvén wings within the main Alfvén wing. These additional smaller wings, so-called Alfvén winglets, develop at the location of the electron beams. They possess the same positive and negative ΔB_x dependence as the main wing. Such Alfvén winglets have been previously reported in the literature, for example, Roth et al. (2011) showed the development of an Alfvén winglet within the main Alfvén wing around the plume of the Tvashtar volcano at Io, and Blöcker et al. (2016) found that an Alfvén winglet is generated within Europa's main wing when local inhomogeneities are present in the atmosphere.

Figure 11 shows the v_x component in the equatorial plane for these two model runs with a simplified setup. In both panels, the plasma flow is diverted around Europa and at the flanks of the main Alfvén wings, reaching speeds of $\sim$120 km s^{-1}. The plasma velocity is slowed down upstream of the moon and reaccelerated downstream. When

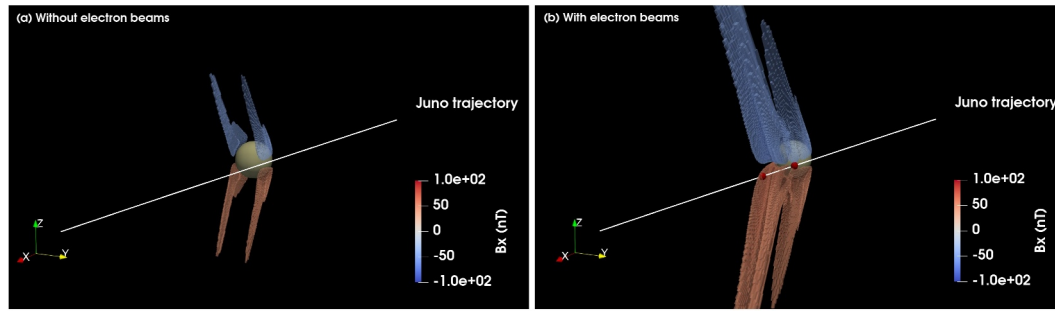

Figure 10. Visualization of the modeled magnetic field B_x component: (a) before and (b) after including electron beams, while all other parameters stay the same. The points in red in panel (b) represent the seed points used for tracing the sheets of beamed electrons for Beams 1 and 2.

we include Beams 1 and 2 in our setup (panel (b)), the plasma flow is further decelerated downstream of Europa along the streamlines from which we trace the sheets of both beams, that is, where the Alfvén winglets develop. The factor $\bar{\alpha} = 1 - v/v_0$ characterizes the relative strength of the sub-Alfvénic interaction (Saur et al., 2013). When $\bar{\alpha} = 0$ the obstacle does not perturb the plasma flow, whereas $\bar{\alpha} = 1$ implies that the interaction is saturated and the plasma flow is halted in the vicinity of the obstacle. The interaction strength in the Alfvén winglet at the location of Beam 1 is much higher $(\bar{\alpha} \sim 0.9)$ than in the surrounding main Alfvén wing $(\bar{\alpha} \sim 0.36)$. Within the winglet developed due to Beam 1, the magnitude of the v_x component is reduced down to $\sim$10 km s^{-1}.

As Figures 10 and 11 demonstrate, the interaction between Europa's atmosphere and its environment generates magnetic field and plasma flow perturbations that propagate as Alfvén waves along the main Alfvén wing. These perturbations are primarily caused by electron impact ionization and elastic collisions between ions and neutrals. In addition, the electron beams lead to locally enhanced ionization of the moon's atmosphere and they further slow down the flow. This results in stronger perturbations that also propagate along the magnetic field lines, which are the main cause for the development of the above-mentioned Alfvén winglets.

4. Discussion of the Flyby Simulation Results

In this work we use an MHD code to model the plasma interaction between Europa and the Jovian magnetosphere for the conditions of the Juno flyby. Our simulations show that we require: (a) a sub-Jovian/anti-Jovian asymmetric O_2 atmosphere, (b) a non-uniform background electron impact ionization frequency, and (c) locally

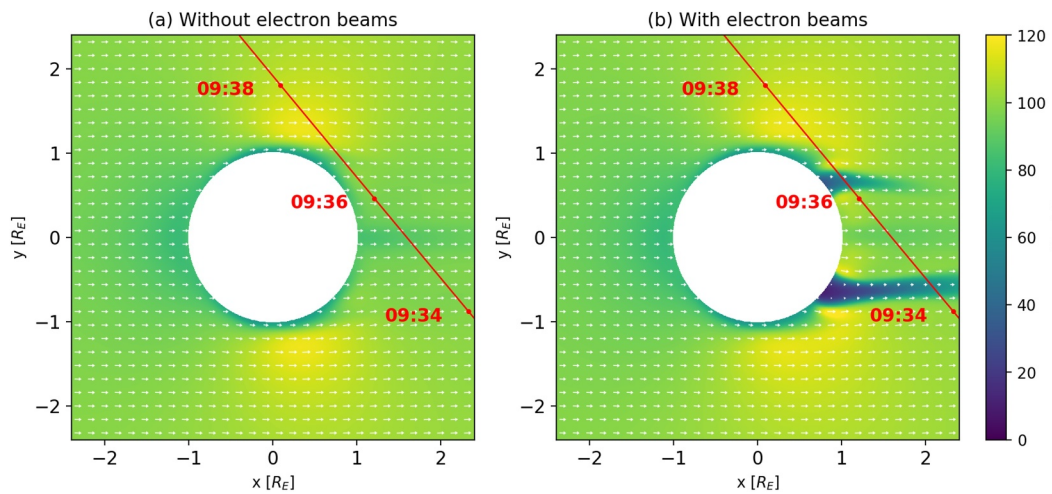

Figure 11. Plasma flow v_x component in the equatorial plane: (a) before and (b) after including electron beams, while all other parameters stay the same. The red line shows Juno's flyby trajectory projected onto this plane. The arrows show the orientation of the plasma flow, and their lengths scale linearly with the maximum magnitude of the velocity in this plane: (a) 117 km s^{-1} and (b) 124 km s^{-1}.

enhanced ionization due to electron beams, in order to produce magnetic field signatures in agreement with the magnetometer onboard Juno, as well as profiles of electron impact ionization frequency and of total ion number density consistent with plasma measurements from the JADE detector. In this section, we assess each of these assumptions, and we discuss alternative scenarios that might also provide an explanation to the spacecraft data.

As mentioned in Section 3.1, based on the pattern of the measured magnetic field, we split this flyby into two time intervals roughly separated around 09:36:00 UTC. The first segment (in the anti-Jovian hemisphere) is dominated by the interaction between Europa's atmosphere and the ambient plasma, whereas the second interval (in the sub-Jovian hemisphere) shows clear signatures of the moon's induced dipole. Hence, we suggest that an asymmetric plasma interaction scenario might have been present at Europa's location at the time of the Juno flyby. One possible way to account for such an asymmetric interaction is by gradually reducing the O_2 column density from the anti-Jovian to the sub-Jovian apex in our model, which given the conditions for this flyby, roughly coincide with the dusk and dawn apexes, respectively. With this asymmetric atmosphere we are able to reproduce, in general, the magnetometer and plasma measurements, and thus our results are indicative that such an asymmetric distribution of O_2 might develop around Europa. However, other magnetospheric effects during the time of the flyby, for example, flux tube interchange or waves generated by enhanced pickup in the wake of Europa, could also affect the observed magnetic field. Both effects were present during the E04 flyby of Galileo (M. G. Kivelson et al., 2009), which followed a very similar trajectory to the Juno flyby, approaching Europa from its anti-Jovian side while traveling upstream, but remaining downstream of the moon for most of the encounter. Therefore, the magnetometer data must be interpreted with caution, and it is not possible to derive a rigorous conclusion about any dawn/dusk asymmetry in Europa's atmosphere at the time of the Juno encounter. Further flybys with a similar trajectory will clarify this question and provide in-situ evidence for the existence of such an asymmetry in the distribution of O_2 around the moon.

Features of a confined nature, which exhibit localized signatures in the magnetic field and plasma data, have been reported previously in the literature. Jia et al. (2018) showed that a sudden, short time-scale fluctuation in the magnetometer and plasma wave data could be explained with the passage of Galileo through a water plume during its E12 flyby. However, none of the instruments onboard Juno revealed evidence of water plumes along the spacecraft trajectory. A second localized feature is the presence of water concentrated around the subsolar point, the presence of which was reported by Roth (2021) on the basis of an analysis of HST images. Building upon the findings of Roth (2021), Cervantes and Saur (2022) inspected the magnetic field measurements of the E12 flyby and, using an MHD model, found a substructure of confined nature coincident with a local maximum in the B_x component. The authors ascribed this localized perturbation to the presence of stable water vapor strongly confined around the subsolar point. Nevertheless, as seen in Figure 1, for the conditions of the Juno flyby, the subsolar point was nearly aligned with the direction of the incident magnetospheric plasma, while the spacecraft was mostly located downstream during its encounter with Europa. Therefore, the stable water component is too far from the trajectory to produce a signature in the plasma interaction. As a consequence, we rule out both localized features as possible explanations to the magnetic field and plasma density measurements during the Juno flyby.

An alternative scenario that might also result in an asymmetric plasma interaction is the ionospheric Hall effect, which is not included in our MHD model. As shown by Saur et al. (1998), the Hall term introduces a slight asymmetry of the plasma flow with respect to the XZ plane (i.e., between the sub-Jovian and anti-Jovian hemispheres). The electron temperature exhibits such asymmetry as well, with larger values in the anti-Jovian half space compared to the sub-Jovian side. Saur et al. (1998) demonstrated that the electron temperature of the thermal population ($T_e = 20$ eV) decreases down to ~16 eV in the anti-Jovian hemisphere, while in the sub-Jovian it reaches a minimum of ~8 eV, with the suprathermal population showing a similar behavior. Given the strong dependence of the electron impact ionization frequency on the electron temperature, an asymmetric background ionization frequency that decreases from the anti-Jovian to the sub-Jovian hemisphere of Europa is a plausible scenario. This, in turn, is consistent with our expectation of plasma interaction effects being dominant in the first part of the flyby and weaker in the second segment.

As mentioned in the previous paragraph, our simulations do not account for the Hall effect. One possible way to incorporate this term in our MHD model, without explicitly including it in the induction Equation 3, is by introducing an asymmetry in the non-uniform background electron impact ionization frequency, such that it resembles the pattern of the asymmetric distribution of electron temperature from Saur et al. (1998). As our

comparison of Runs 2 and 3 has evidenced, the spatial structure of the background ionization frequency has a clear effect on the magnetic field and plasma perturbations around Europa. It will be subject of future work to further investigate the effects of such an asymmetric ionization on the plasma interaction.

The inclusion of electron beams in our MHD model relies on a number of assumptions and arbitrary constraints. First of all, we consider that the electron beams are ducted along the magnetic field lines, and as they are advected downstream of Europa, they trace two-dimensional sheets. In addition, we assume a Gaussian in order to describe the spatial distribution of the enhanced impact ionization perpendicular to the sheets. Several parameters of the sheets, such as the coordinates of the seed points, the maximum ionization frequency along each sheet, and the width of the Gaussians, are constrained by the electron impact ionization rates inferred from JADE electron measurements. The extent of the sheets, both along the velocity streamlines and the magnetic field lines, is currently unconstrained, and we arbitrarily extend them 4 R_E downstream, noting that the role of the beams is negligible where the atmospheric density vanishes. Additional flybys, upstream of the trajectory of Juno, as well as further downstream in the wake, will provide further characterization of the spatial structure of the sheets and their enhanced ionization.

Our MHD simulations show that the electron beams have two clear effects on Europa's plasma environment. First of all, the beams contribute to perturbations in the magnetic field components throughout the region where they are observed. As our results indicate, the increase in ionization produces sudden bumps in the B_x component (especially at the location of Beams 1 and 2), and the general structure of enhancements and dips of B_x throughout the geometric wake. The small-scale fluctuations visible in the data on top of the main perturbations could be related to the presence of waves and instabilities downstream of the moon, which our model does not account for. The second effect of the electron beams is to fill the wake with newly ionized plasma, and thus our MHD simulations are consistent with the observations by Allegrini et al. (2024a) that show high values of electron density in the same region. This is in contrast to previous numerical studies that do not account for the presence of the beams (e.g., Blöcker et al., 2016; Harris et al., 2022; Saur et al., 1998), and as a result, yield simulations with an empty or a partially empty wake.

The electron beams enter our MHD model through locally enhancing the electron impact ionization, which leads to an increase in plasma mass loading and a reduction of the plasma bulk velocity in Europa's vicinity. This results in the development of Alfvén winglets at the location of the beams. In addition, as mentioned by Allegrini et al. (2024a), an imbalance between the parallel and antiparallel fluxes at Beams 1 and 2 causes net electric currents. This implies that the electron beams might contribute to the electric current system connecting the moon's ionosphere with its Alfvén wings. These currents might, in turn, contribute to the measured magnetic field perturbations.

The possible role of the beams in carrying net electric current could provide an explanation to the apparent misfit between the observed and modeled ion density due to Beam 1. As our Run 5 has shown, we overpredict the plasma density at the location of this beam, and as a consequence, we might also overestimate the resulting effects of the ionization on the magnetic field. If magnetic field perturbations collocated with electron beams are partially caused by electric currents flowing along them, such currents would generate larger jumps in the modeled magnetic field without the need for larger values in the ion density. This suggests that the magnetic field perturbations might not be in their entirety due to the ionizing effect of the beams, but rather partially due to electric currents in the beams as well. However, such a possible role of the beams in carrying electric current and the resulting effects on the magnetic field data are not accounted for in our MHD model.

Finally, our implementation of the electron beams in the code is performed in a not self-consistent way, as we keep the spatial structure of the sheets of enhanced ionization constant throughout the simulation. However, as the plasma flow is advected downstream of the moon, the structure of the sheets might be time-variable. Our current approach represents a first step towards modeling and understanding the key role of the electron beams in shaping Europa's plasma environment, and further refinement of our implementation of the beams in the model will be subject of future work.

5. Concluding Remarks

In this study, we use an MHD model to simulate the interaction between Europa's atmosphere and Jupiter's magnetosphere for the conditions of the Juno flyby. We compare our predicted magnetic field and total ion

number density to the magnetometer and JADE plasma observations, respectively. In particular, we focus on the effect of three properties on the plasma interaction: (a) an O_2 atmosphere with a sub-Jupiter/anti-Jupiter asymmetry, (b) a non-uniform distribution of the background electron impact ionization, and (c) localized enhanced ionization due to electron beams in the moon's geometric wake.

One important feature of this flyby is that the magnetometer data shows signatures of Europa's induced field dominating after time of CA in the sub-Jovian hemisphere of the moon. This implies that the contribution of plasma interaction effects to the measured field gradually decreases as Juno travels towards Jupiter. We account for this scenario by introducing in our MHD model an asymmetric distribution of O_2 around the moon in the Jupiter direction, which given the characteristics of this flyby, roughly coincides with a dusk/dawn asymmetry. Our results are indicative that this asymmetric atmosphere might be present around the moon. Additional flybys with a similar trajectory in Europa's dusk and dawn hemispheres are needed to further clarify the existence of such an atmospheric asymmetry. However, we emphasize that other processes could also result in an asymmetric plasma interaction, for example, the Hall effect which slightly perturbs the flow in the Jupiter direction and introduces an asymmetry on the electron temperature. This could lead to an asymmetric distribution of the background electron impact ionization frequency, and thus, in plasma interaction effects that decrease in the above-mentioned direction.

We include the electron beams as sheets of enhanced ionization downstream of Europa at the locations where Juno detected them, following the observations by Allegrini et al. (2024a), and we use the profile of electron impact ionization frequency of O_2 from Szalay et al. (2024) to constrain the parameters of the sheets. We specifically focus on the effect of the enhanced ionization due to the beams on the plasma density and the magnetic field. Our MHD simulations prove that the electron beams have an outsize influence on the plasma interaction at Europa by filling the wake downstream of the moon and by producing large perturbations of the magnetic field which appear to contribute to the magnetic field data. The electron beams ionize the neutral gas along their path, and as a consequence, the increased mass loading reduces the plasma flow around the moon. This leads to the development of Alfvén winglets at the location of the beams. Other possible effects of the electron beams on the magnetic field which are not included in our MHD model, for example, by carrying net electric current, might also contribute to the observed magnetic field perturbations. Our study constitutes a first step towards understanding the influence of the electron beams in Europa's plasma interaction, and it presents a scenario for the conditions of the Juno flyby which might explain the magnetometer and plasma observations.

The amplitudes of the magnetic field perturbations generated by the electron beams are on the order of ∼50–100 nT in our model results. These amplitudes are similar to the signatures of the moon's induced field. Therefore, the electron beams need to be thoroughly understood and accounted for in future attempts to diagnose Europa's subsurface water ocean. Our findings provide both the JUICE (Grasset et al., 2013) and Europa Clipper (Howell & Pappalardo, 2020) mission teams with valuable information on the location and ionization rates of these beams, as well as on their associated magnetic field signatures. In situ magnetic field and plasma measurements will further refine our characterization of the electron beams and will advance our understanding of their key role in shaping Europa's space plasma environment.

Data Availability Statement

The PLUTO code (Mignone et al., 2007) utilized in this work is open-source and can be downloaded from https://plutocode.ph.unito.it/download.html (version 4.4). The complete simulation output for the five MHD Runs 1 to 5 are available at a Zenodo repository via https://doi.org/10.5281/zenodo.13939163 with CCA 4.0 license (Cervantes et al., 2025b). The predicted magnetic field, electron impact ionization frequency, and total ion number density along Juno's trajectory from the five MHD Runs 1 to 5 are available at a Zenodo repository via https://doi.org/10.5281/zenodo.14825144 with CCA 4.0 license (Cervantes et al., 2025a). The JNO-J-3-FGM-CAL-V1.0 magnetic field data (Connerney, 2024) collected by Juno's magnetometer (Connerney et al., 2017) was retrieved from the NASA Planetary Data System (PDS) at https://pds-ppi.igpp.ucla.edu/collection/JNO-J-3-FGM-CAL-V1.0:DATA. The values for the electron impact ionization frequency of O_2 and the total ion number density derived from JADE plasma measurements (McComas et al., 2017) were obtained from the Source Data for Figure 1 in Szalay et al. (2024). The electron data shown in the spectrograms in the top two panels of Figure 3 was sourced from Allegrini et al. (2024b).

Acknowledgments
The work at the University of Cologne has received funding from the European Research Council (ERC) under the European Union's Horizon 2020 research and innovation programme (grant agreement no. 884711). This work used resources of the Deutsches Klimarechenzentrum (DKRZ) granted by its Scientific Steering Committee (WLA) under project ID 1350. We also thank the Regional Computing Center of the University of Cologne (RRZK) for computing time on the High Performance Computing system CHEOPS. The work of S. Cervantes at DIAS was supported by Taighde Éireann - Research Ireland award 22/FFP-P/11545.

References

Addison, P., Haynes, C. M., Stahl, A. M., Liuzzo, L., & Simon, S. (2024). Magnetic signatures of the interaction between Europa and Jupiter's magnetosphere during the Juno flyby. *Geophysical Research Letters*, *51*(2), e2023GL106810. https://doi.org/10.1029/2023gl106810

Allegrini, F., Saur, J., Szalay, J., Ebert, R., Kurth, W., Cervantes, S., et al. (2024b). Electron beams at Europa (dataset). *Zenodo*. https://doi.org/10.5281/zenodo.10974579

Allegrini, F., Saur, J., Szalay, J., Ebert, R., Kurth, W., Cervantes, S., et al. (2024a). Electron beams at Europa. *Geophysical Research Letters*, *51*(13), e2024GL108422. https://doi.org/10.1029/2024gl108422

Arnold, H., Liuzzo, L., & Simon, S. (2019). Magnetic signatures of a plume at Europa during the Galileo E26 flyby. *Geophysical Research Letters*, *46*(3), 1149–1157. https://doi.org/10.1029/2018gl081544

Bagenal, F., & Dols, V. (2020). The space environment of Io and Europa. *Journal of Geophysical Research: Space Physics*, *125*(5), e2019JA027485. https://doi.org/10.1029/2019ja027485

Blöcker, A., Saur, J., & Roth, L. (2016). Europa's plasma interaction with an inhomogeneous atmosphere: Development of Alfvén winglets within the Alfvén wings. *Journal of Geophysical Research: Space Physics*, *121*(10), 9794–9828. https://doi.org/10.1002/2016ja022479

Bolton, S. J., Lunine, J., Stevenson, D., Connerney, J., Levin, S., Owen, T., et al. (2017). The Juno mission. *Space Science Reviews*, *213*, 5–37. https://doi.org/10.1007/978-94-024-1560-5_2

Cervantes, S., & Saur, J. (2022). Constraining Europa's subsolar atmosphere with a joint analysis of HST spectral images and Galileo magnetic field data. *Journal of Geophysical Research: Space Physics*, *127*(9), e2022JA030472. https://doi.org/10.1029/2022ja030472

Cervantes, S., Saur, J., Duling, S., Szalay, J., Schlegel, S., Connerney, J., et al. (2025a). MHD model of Europa's plasma interaction: Model output along the trajectory of Juno (dataset). *Zenodo*. Retrieved from https://doi.org/10.5281/zenodo.14825144

Cervantes, S., Saur, J., Duling, S., Szalay, J., Schlegel, S., Connerney, J., et al. (2025b). MHD model output of Europa's plasma interaction during the Juno flyby (dataset). *Zenodo*. Retrieved from https://doi.org/10.5281/zenodo.13939163

Connerney, J. (2024). *Juno MAG CALIBRATED DATA J V1.0, JNO-J-3-FGM-CAL-V1.0 (dataset)*. NASA Planetary Data System. Retrieved from https://pds-ppi.igpp.ucla.edu/collection/JNO-J-3-FGM-CAL-V1.0

Connerney, J., Benn, M., Bjarno, J., Denver, T., Espley, J., Jorgensen, J., et al. (2017). The Juno magnetic field investigation. *Space Science Reviews*, *213*(1–4), 39–138. https://doi.org/10.1007/s11214-017-0334-z

Duling, S., Saur, J., Clark, G., Allegrini, F., Greathouse, T., Gladstone, R., et al. (2022). Ganymede MHD model: Magnetospheric context for Juno's PJ34 flyby. *Geophysical Research Letters*, *49*(24), e2022GL101688. https://doi.org/10.1029/2022gl101688

Duling, S., Saur, J., & Wicht, J. (2014). Consistent boundary conditions at nonconducting surfaces of planetary bodies: Applications in a new Ganymede MHD model. *Journal of Geophysical Research: Space Physics*, *119*(6), 4412–4440. https://doi.org/10.1002/2013ja019554

Frank, L., & Paterson, W. (1999). Intense electron beams observed at Io with the Galileo spacecraft. *Journal of Geophysical Research*, *104*(A12), 28657–28669. https://doi.org/10.1029/1999ja900402

Goertz, C. (1980). Io's interaction with the plasma torus. *Journal of Geophysical Research*, *85*(A6), 2949–2956. https://doi.org/10.1029/ja085ia06p02949

Grasset, O., Dougherty, M., Coustenis, A., Bunce, E., Erd, C., Titov, D., et al. (2013). JUpiter ICy moons Explorer (JUICE): An ESA mission to orbit Ganymede and to characterise the Jupiter system. *Planetary and Space Science*, *78*, 1–21. https://doi.org/10.1016/j.pss.2012.12.002

Harris, C. D., Jia, X., & Slavin, J. A. (2022). Multi-fluid MHD simulations of Europa's plasma interaction: Effects of variation in Europa's atmosphere. *Journal of Geophysical Research: Space Physics*, *127*(9), e2022JA030569. https://doi.org/10.1029/2022ja030569

Harris, C. D., Jia, X., Slavin, J. A., Toth, G., Huang, Z., & Rubin, M. (2021). Multi-fluid MHD simulations of Europa's plasma interaction under different magnetospheric conditions. *Journal of Geophysical Research: Space Physics*, *126*(5), e2020JA028888. https://doi.org/10.1029/2020ja028888

Howell, S., & Pappalardo, R. (2020). NASA's Europa clipper—A mission to a potentially habitable ocean world. *Nature Communications*, *11*(1), 1–4. https://doi.org/10.1038/s41467-020-15160-9

Huebner, W. F., Keady, J. J., & Lyon, S. (1992). *Solar photo rates for planetary atmospheres and atmospheric pollutants*. Springer.

Jia, X., Kivelson, M. G., Khurana, K. K., & Kurth, W. S. (2018). Evidence of a plume on Europa from Galileo magnetic and plasma wave signatures. *Nature Astronomy*, *2*(6), 459–464. https://doi.org/10.1038/s41550-018-0450-z

Kabin, K., Combi, M., Gombosi, T., Nagy, A., DeZeeuw, D., & Powell, K. (1999). On Europa's magnetospheric interaction: A MHD simulation of the E4 flyby. *Journal of Geophysical Research*, *104*(A9), 19983–19992. https://doi.org/10.1029/1999ja900263

Khurana, K., Kivelson, M., Stevenson, D., Schubert, G., Russell, C., Walker, R., & Polanskey, C. (1998). Induced magnetic fields as evidence for subsurface oceans in Europa and Callisto. *Nature*, *395*(6704), 777–780. https://doi.org/10.1038/27394

Kivelson, M., Bagenal, F., Kurth, W. S., Neubauer, F. M., Paranicas, C., & Saur, J. (2004). Magnetospheric interactions with satellites. *Jupiter: The planet, satellites and magnetosphere*, 513–536.

Kivelson, M. G., Khurana, K. K., & Volwerk, M. (2009). Europa's interaction with the Jovian magnetosphere. Europa (pp. 545–570).

Kurth, W., Hospodarsky, G., Kirchner, D., Mokrzycki, B., Averkamp, T., Robison, W., et al. (2017). The Juno waves investigation. *Space Science Reviews*, *213*(1–4), 347–392. https://doi.org/10.1007/s11214-017-0396-y

Kurth, W., Wilkinson, D. R., Hospodarsky, G. B., Santolik, O., Averkamp, T. F., Sulaiman, A. H., et al. (2023). Juno plasma wave observations at Europa. *Geophysical Research Letters*, *50*(24), e2023GL105775. https://doi.org/10.1029/2023gl105775

McComas, D., Alexander, N., Allegrini, F., Bagenal, F., Beebe, C., Clark, G., et al. (2017). The Jovian auroral distributions experiment (JADE) on the Juno mission to Jupiter. *Space Science Reviews*, *213*(1–4), 547–643. https://doi.org/10.1007/s11214-013-9990-9

McGrath, M., Lellouch, E., Strobel, D. F., Feldman, P. D., & Johnson, R. E. (2004). Satellite atmospheres. *Jupiter: The planet, satellites and magnetosphere*, 457–483.

Mignone, A., Bodo, G., Massaglia, S., Matsakos, T., Tesileanu, O. E., Zanni, C., & Ferrari, A. (2007). Pluto: A numerical code for computational astrophysics. *The Astrophysical Journal - Supplement Series*, *170*(1), 228–242. https://doi.org/10.1086/513316

Neubauer, F. (1980). Nonlinear standing Alfvén wave current system at Io: Theory. *Journal of Geophysical Research*, *85*(A3), 1171–1178. https://doi.org/10.1029/ja085ia03p01171

Neubauer, F. (1998). The sub-Alfvénic interaction of the Galilean satellites with the Jovian magnetosphere. *Journal of Geophysical Research*, *103*(E9), 19843–19866. https://doi.org/10.1029/97je03370

Neubauer, F. (1999). Alfvén wings and electromagnetic induction in the interiors: Europa and callisto. *Journal of Geophysical Research*, *104*(A12), 28671–28684. https://doi.org/10.1029/1999ja900217

Plainaki, C., Cassidy, T. A., Shematovich, V. I., Milillo, A., Wurz, P., Vorburger, A., et al. (2018). Towards a global unified model of Europa's tenuous atmosphere. *Space Science Reviews*, *214*(1), 1–71. https://doi.org/10.1007/s11214-018-0469-6

Roth, L. (2021). A stable H2O atmosphere on Europa's trailing hemisphere from HST images. *Geophysical Research Letters*, *48*(20), e2021GL094289. https://doi.org/10.1029/2021gl094289

Roth, L., Saur, J., Retherford, K. D., Strobel, D. F., Feldman, P. D., McGrath, M. A., et al. (2016). Europa's far ultraviolet oxygen aurora from a comprehensive set of HST observations. *Journal of Geophysical Research: Space Physics*, *121*(3), 2143–2170. https://doi.org/10.1002/2015ja022073

Roth, L., Saur, J., Retherford, K. D., Strobel, D. F., & Spencer, J. R. (2011). Simulation of Io's auroral emission: Constraints on the atmosphere in eclipse. *Icarus*, *214*(2), 495–509. https://doi.org/10.1016/j.icarus.2011.05.014

Rubin, M., Jia, X., Altwegg, K., Combi, M., Daldorff, L., Gombosi, T., et al. (2015). Self-consistent multifluid MHD simulations of Europa's exospheric interaction with Jupiter's magnetosphere. *Journal of Geophysical Research: Space Physics*, *120*(5), 3503–3524. https://doi.org/10.1002/2015ja021149

Saur, J. (2021). Overview of moon–magnetosphere interactions. *Magnetospheres in the Solar System*, 575–593. https://doi.org/10.1002/9781119815624.ch36

Saur, J., Grambusch, T., Duling, S., Neubauer, F., & Simon, S. (2013). Magnetic energy fluxes in sub-Alfvénic planet star and moon planet interactions. *Astronomy and Astrophysics*, *552*, A119. https://doi.org/10.1051/0004-6361/201118179

Saur, J., Neubauer, F. M., & Glassmeier, K.-H. (2010). Induced magnetic fields in Solar System bodies. *Space Science Reviews*, *152*(1), 391–421. https://doi.org/10.1007/s11214-009-9581-y

Saur, J., Strobel, D., & Neubauer, F. (1998). Interaction of the jovian magnetosphere with Europa: Constraints on the neutral atmosphere. *Journal of Geophysical Research*, *103*(E9), 19947–19962. https://doi.org/10.1029/97je03556

Saur, J., Strobel, D. F., Neubauer, F. M., & Summers, M. E. (2003). The ion mass loading rate at Io. *Icarus*, *163*(2), 456–468. https://doi.org/10.1016/s0019-1035(03)00085-x

Schilling, N., Khurana, K., & Kivelson, M. (2004). Limits on an intrinsic dipole moment in Europa. *Journal of Geophysical Research*, *109*(E5). https://doi.org/10.1029/2003je002166

Schilling, N., Neubauer, F., & Saur, J. (2007). Time-varying interaction of Europa with the jovian magnetosphere: Constraints on the conductivity of Europa's subsurface ocean. *Icarus*, *192*(1), 41–55. https://doi.org/10.1016/j.icarus.2007.06.024

Schilling, N., Neubauer, F., & Saur, J. (2008). Influence of the internally induced magnetic field on the plasma interaction of Europa. *Journal of Geophysical Research*, *113*(A3). https://doi.org/10.1029/2007ja012842

Schunk, R., & Nagy, A. (2009). *Ionospheres: Physics, plasma physics, and chemistry*. Cambridge University Press.

Szalay, J., Allegrini, F., Ebert, R., Bagenal, F., Bolton, S., Fatemi, S., et al. (2024). Oxygen production from dissociation of Europa's water-ice surface. *Nature Astronomy*, 1–10.

Volwerk, M., Khurana, K., & Kivelson, M. (2007). Europa's Alfvén wing: Shrinkage and displacement influenced by an induced magnetic field. *Annales Geophysicae*, *25*(4), 905–914. https://doi.org/10.5194/angeo-25-905-2007

Williams, D., Mauk, B., McEntire, R., Roelof, E., Armstrong, T., Wilken, B., et al. (1996). Electron beams and ion composition measured at Io and in its torus. *Science*, *274*(5286), 401–403. https://doi.org/10.1126/science.274.5286.401

Zimmer, C., Khurana, K. K., & Kivelson, M. G. (2000). Subsurface oceans on Europa and callisto: Constraints from Galileo magnetometer observations. *Icarus*, *147*(2), 329–347. https://doi.org/10.1006/icar.2000.6456